

Development of an Electropolishing Method for Titanium Materials

Alexandre Faria Teixeira

A Thesis

In

The Department

of

Mechanical and Industrial Engineering

Presented in Partial Fulfillment of the Requirements  
For the Degree of Master of Applied Science (Mechanical Engineering) at  
Concordia University  
Montreal, Quebec, Canada

March 2011

© Alexandre Faria Teixeira, 2011

**CONCORDIA UNIVERSITY**

**School of Graduate Studies**

This is to certify that the thesis prepared

By: Alexandre Faria Teixeira

Entitled: Development of an Electropolishing Method for Titanium Materials

and submitted in partial fulfillment of the requirements for the degree of

**Master of Applied Science (Engineering)**

complies with the regulations of the University and meets the accepted standards with respect to originality and quality.

Signed by the final examining committee:

----- Dr. Ming Chen	Chair
----- Dr. Lyes Kadem	Examiner
----- Dr. Rolf Wuthrich	Examiner/Supervisor
----- Dr. Sasha Omanovic	Examiner

Approved by:

-----  
Chair of Department or Graduate Program Director

-----  
Dean of Faculty

## ABSTRACT

Development of an Electropolishing Method for Titanium Materials

Alexandre Faria Teixeira

The objective of this research is to develop a new electropolishing (EP) method for titanium (Ti) materials, which will enable a significant roughness reduction of complex parts manufactured by selective laser sintering (SLS). The average surface finish should be 3Sa or less in an area of 640 x 480  $\mu\text{m}$ , regardless of the initial conditions, with low metal removal.

The research studies a promising method that could overcome two major deficiencies of traditional EP techniques: (1) the dependence on initial conditions to achieve satisfactory surface finishes, and (2) the use of toxic electrolytes, which are often applied when dealing with titanium.

Current EP techniques are not able to systematically improve surface finishes. Specialized companies advertise a possible reduction of only up to 50% in roughness profilometer readings. This implies that parts with very rough initial conditions must be submitted to other polishing methods prior to EP for satisfactory results. However, in many cases, other polishing techniques are either too costly or are not suitable for the geometric complexity of the parts. Regarding the environment, the use of a less toxic electrolyte for Ti, which currently employs very acidic and aggressive solutions, will address the growing demand for cleaner and safer technologies.

SLS is a manufacturing technique recommended for machining complex shapes of various types of materials, from nylon to metals. This process, when used with Ti, results in a very rough surface finish. A more efficient EP method should be able to improve the

performance of the parts in a wide range of applications, while keeping the overall cost competitive. The results of this research proved to be promising both in terms of efficiency and impact on the environment. By using NaCl-ethylene glycol as an electrolyte and electric pulses as opposed to direct current, surface roughnesses were reduced by 50-70 per cent. Moreover, if the pulse technology parameters are optimized, there is a great potential to achieve even better results.

This research was developed in association with DynaTool Industries, headquartered in Montreal, Quebec. DynaTool Industries seeks a process to complement its SLS line of production, as none of the existing methods in industry are able to satisfy its requirements and specifications. DynaTool Industries invests in research to achieve superb technology enhancing the value of its products.

# Table of Contents

List of Figures..... vii  
List of Tables..... ix

## Chapters

**1. Introduction ..... 1**

1.1. Selective Laser Sintering ..... 2

1.2. Titanium ..... 3

1.2.1. Characteristics ..... 3

1.2.2. Stability of Molecules ..... 5

1.2.3. Oxide Layer ..... 5

1.3. Conventional Polishing Techniques ..... 6

1.3.1. Abrasive Techniques..... 6

1.3.2. Large Area Electron Beam Irradiation ..... 7

1.3.3. Electropolishing ..... 8

**2. Electropolishing ..... 10**

2.1. Theoretical Background ..... 11

2.2. Mass Transport Mechanisms ..... 12

2.2.1. The Duplex Salt Film: ..... 13

2.2.2. Adsorbate Acceptor Model: ..... 14

2.3. Diffusion and the Nernst Diffusion Layer ..... 14

2.4. Rate of Dissolution and Current Density..... 16

2.5. Characterization of the Nernst Diffusion Layer Evolution..... 21

2.6. Limitations of Traditional EP ..... 25

2.7. Modeling Mechanism for the Pulse Technology..... 26

**3. The use of Ethylene Glycol in Electropolishing of Titanium Materials ..... 31**

3.1. Ethylene Glycol ..... 32

3.2. Electrochemical Behaviour of Ethylene Glycol ..... 32

3.3. Possible Reactions in the Process.....	33
3.3.1. Substances Involved .....	33
3.3.2. Dissolution of the Electrolyte .....	34
3.3.3. Thermodynamic Data .....	34
3.3.4. Anode: Possible Reactions.....	35
3.3.5. Cathode: Possible Reactions.....	39
3.4. Determination of the Dissociation Valence of Titanium.....	40
3.5. Rotating Disk Electrode Experiments .....	41
3.6. Variation with Temperature.....	42
3.7. Experiments Varying Concentration of Cl <sup>-</sup> Anions.....	44
3.8. Variation of the Concentration of Ti Cations in the Bulk Solution.....	46
3.9. Roughness Analysis.....	47
<b>4. Application of the Pulse Technology.....</b>	<b>50</b>
4.1. Formation of the Oxide Layer under Normal Conditions .....	51
4.2. High Level Temperature Issue .....	52
4.3. Apparatus to Create an Inert Environment and Monitor Key Process Variables .....	55
4.4. Results Obtained.....	58
4.5. Variation of Time .....	61
4.6. Variation of Pulse Width .....	62
4.7. Variation of Duty Cycle .....	64
4.8. Conclusions .....	66
<b>5. Conclusions, Original Contributions to Knowledge and Future Prospects.....</b>	<b>67</b>
5.1. The Pulse Technology .....	68
5.2. Conclusions and Original Contributions to Knowledge.....	69
5.3. Ideas for Future Work .....	70
<b>References.....</b>	<b>71</b>
<b>Appendix.....</b>	<b>74</b>

## List of Figures

Figure 1-1 - Selective Laser Sintering Apparatus [13].	3
Figure 1-2 - Abrasive Polishing of a Metal Plate [19].	7
Figure 1-3 - Large Area Electron Beam Irradiation [20].	8
Figure 1-4 - Schematic Illustration of a Typical Electropolishing System.	9
Figure 2-1 - Schematic Illustration of a Typical Electropolishing System.	11
Figure 2-2 - Duplex Salt Film Transport Mechanism [25].	13
Figure 2-3 - Adsorbate Acceptor Model Transport Mechanism [25].	14
Figure 2-4 - Depiction of the Nernst Diffusion Layer.	15
Figure 2-5 - Current Density Ratio x Asperity Size at Different Times.	19
Figure 2-6 - Time Evolution of Ratio Between Spherical and Linear Diffusion.	20
Figure 2-7 - First Stage: Nernst Diffusion Layer Evolution with Time.	22
Figure 2-8 - Second Stage: Nernst Diffusion Layer Evolution with Time.	23
Figure 2-9 - Third Stage: Nernst Diffusion Layer Evolution with Time.	24
Figure 3-1 - Ethylene Glycol Molecule.	32
Figure 3-2 - Voltammogram of the Electrochemical Behaviour of Ethylene Glycol [29].	33
Figure 3-3 - Ti Being Electropolished. Gas Evolution Occurring in Counter and Working Electrodes.	36
Figure 3-4 - Comparison Between Polishing Results with a Low Duty Cycle (left) and a High Duty Cycle (right).	37
Figure 3-5 - Comparison Between Polishing Results with Low Duty Cycles, and a High Oxygen Level (left) and a Low Oxygen Level (right).	38
Figure 3-6 - Titanium Piece with Tip Electropolished.	39
Figure 3-7 - Current Transient during Anodic Polarization of Ti at 15V in 1M Ethylene Glycol Solution [17].	41
Figure 3-8 - Anodic Polarization Curves Using a Ti Rotating Disk.	42
Figure 3-9 - Current x Temp. Plot of Ti Electropolishing at 15V	43
Figure 3-10 - Potential-Independent Current $i_{limit}$ as a Function of Square Root of Angular Velocity in LiCl Ethylene Glycol Solution [28].	44
Figure 3-11- Koutecky-Levich Plot, $i_{limit}^{-1}$ as a Function of $w^{-1/2}$ , in LiCl Ethylene Glycol Solution [28].	45
Figure 3-12 - Relation Between Current Density in the Absence of any Mass Transfer Effect $i_k$ and Solution Conductivity $\lambda$ [28].	46
Figure 3-13 - Levich Plot in LiCl Solution Containing Different Concentrations of Ti Ions [28].	47
Figure 3-14 - Roughness Profiles with Different Methods [17].	47
Figure 3-15 - Roughness Profiles Before and After Electropolishing.	48
Figure 3-16 - Titanium Piece with Tip Electropolished.	48
Figure 4-1 - Ti not Successfully Electropolished with Pulse Technology due to High Oxygen Levels.	51

Figure 4-2 - Side by Side Comparison of the Process with Two Different Setups. The Setup of the Right Leads to Higher Temperatures. Both Pictures were Taken at the Very Beginning of the Process. ....	52
Figure 4-3 - Identical Comparison of Figure 4-2 but 100 Seconds After. ....	53
Figure 4-4 - Identical Comparison of Figure 4-2 but 200 Seconds After. ....	53
Figure 4-5 - Identical Comparison of Figure 4-2 but 300 Seconds After. ....	53
Figure 4-6 - Identical Comparison of Figure 4-2 but 400 Seconds After. ....	54
Figure 4-7 - Identical Comparison of Figure 4-2 but 500 Seconds After. ....	54
Figure 4-8 - Identical Comparison of Figure 4-2 but 600 Seconds After. ....	54
Figure 4-9 - Ti not Successfully Electropolished with Pulse Technology due to High Temperature Levels. ....	55
Figure 4-10 - Electrochemical Cell Designed for Polishing Ti. ....	56
Figure 4-11 - Software Built for New Electrochemical Cell. ....	57
Figure 4-12 - Voltage and Current Values Monitored While Applying Electrical Pulses. ....	58
Figure 4-13 - Titanium Pieces Successfully Electropolished with the Pulse Technology. ....	59
Figure 4-14 - Roughness Profiles of Titanium Electropolished with Direct Current. The Range of Colors Varies from 120 $\mu$ m to 0 $\mu$ m. ....	59
Figure 4-15 - Roughness Profiles of Titanium Electropolished with Pulse Technology. The Range of Colors Varies from 120 $\mu$ m to 0 $\mu$ m. ....	60
Figure 4-16 - Samples Used for Comparison Between Direct Current and Pulse Technology. ....	60
Figure 4-17 - Roughness Profiles of Titanium Electropolished with Pulse Technology Varying Time. The Range of Colors Varies from 120 $\mu$ m to 0 $\mu$ m. ....	61
Figure 4-18 - Variation of Surface Roughness x Time. ....	62
Figure 4-19 - Roughness Profiles of Titanium Electropolished with Pulse Technology Varying Pulse Width. The Range of Colors Goes from 120 $\mu$ m to 0 $\mu$ m. ....	63
Figure 4-20 - Initial Condition for Experiments Varying Pulse Width. The Range of Colors Goes from 120 $\mu$ m to 0 $\mu$ m. ....	63
Figure 4-21 - Sample Used for Comparison Between Pulse Widths. ....	63
Figure 4-22 - Variation of Surface Roughness x Pulse Width. ....	64
Figure 4-23 - Roughness Profiles of Titanium Electropolished with Pulse Technology Varying Duty Cycle. The Range of Colors Goes from 210 $\mu$ m to 0 $\mu$ m. ....	64
Figure 4-24 - Initial Condition for Experiments Varying Duty Cycle. The Range of Colors Goes from 210 $\mu$ m to 0 $\mu$ m. ....	65
Figure 4-25 - Sample Used for Comparison Between Duty Cycles. ....	65
Figure 4-26 - Variation of Surface Roughness x Duty Cycle. ....	66

## List of Tables

Table 1-1 - Titanium Overview .....	3
Table 1-2 - Titanium Atomic Structure .....	4
Table 1-3 - Titanium Chemical Properties .....	4
Table 1-4 - Titanium Physical Properties .....	5
Table 1-5 - Titanium Stability of Molecules [14][15] .....	5
Table 2-1 - Electropolishing Companies .....	26
Table 3-1 - Titanium EP with Ethylene Glycol – Thermodynamic Data of Molecules [30][14] [15] .....	35

## 1. Introduction

Selective Laser Sintering (SLS) is a competitive method for manufacturing highly complex metal pieces such as gears and advanced medical equipment. However, when used with titanium, this technology leaves a poor surface finish. This is a concern since it increases the friction coefficient [1], renders the piece more prone to corrosion [2], affects bacterial colonization [3][4] and hides stress fractures and imperfections. Because of the complex nature of the pieces in which SLS is competitive in manufacturing, traditional abrasive methods for polishing are not viable since a consistent homogenous roughness is not achievable. Abrasive techniques and large area electron beam irradiation are not suitable for the crevasses of the work pieces. Due to these shortcomings, an alternative method will be analyzed: electropolishing (EP). EP is a process that can be characterized as reverse electroplating: instead of plating the work piece, a thin layer is removed from it, effectively polishing it.

Conventionally, EP techniques are not able to effectively polish work pieces with very rough surfaces. Another concern is that the process normally uses toxic, acidic and aggressive electrolytes especially when dealing with titanium. The reason for this choice is that titanium readily forms an oxide layer in the presence of oxygen. Therefore, very strong acids were used as electrolytes to reduce the formation of the oxide layer. Studies have been made using hazardous chemicals such as perchloric [5][6][7], hydrofluoric[8][9], chromic[8], and/or sulfuric acids[9][10][11]. In this study, a less toxic electrolyte was used: ethylene glycol.

## **1.1. Selective Laser Sintering**

Selective Laser Sintering (SLS) is a manufacturing technique that uses a high intensity laser to fuse small particles of metal, plastic, ceramic, or glass powders into a desired shape. It was patented in 1989 by Carl Deckard [12], a graduate student from the University of Texas. As Figure 1-1 illustrates, an SLS machine consists of two powder chambers on both sides of the work area. The levelling roller moves powder over from one magazine, crossing over the work area to the other magazine. The laser then traces out the layer. The work platform moves down by the thickness of one layer and the roller then moves in the opposite direction. The process repeats until the part is complete, layer by layer. The surface of a SLS part is powdery, like the base material, whose particles are fused together without complete melting. In addition, if the temperature of uncured SLS powder gets too high, excess fused material can collect on the part surface. This can be difficult to control since there are many variables in the SLS process. The high surface roughness raises the need for surface polishing, especially if the manufactured part is sensitive to corrosion, fouling, plugging, scaling, product build-up or growth of bacteria.

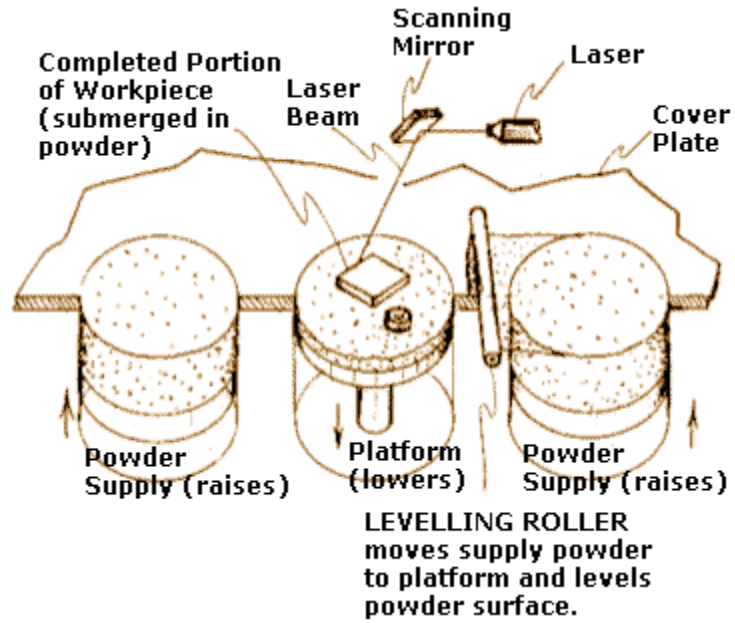


Figure 1-1 - Selective Laser Sintering Apparatus [13].

## 1.2. Titanium

### 1.2.1. Characteristics

Pure titanium is a lustrous white metal, as strong as steel but 45% lighter and 60% heavier than aluminum. The main information regarding its characteristics can be found in Tables 1-1 through 1-4.

Overview	
Atomic Number	22
Group	4
Series	Transition Metals
Period	4

Table 1-1 - Titanium Overview

Atomic Structure	
Atomic Radius	2Å

Atomic Volume	10.64cm <sup>3</sup> /mol
Covalent Radius	1.32Å
Cross Section (Thermal Neutron Capture)	6.09 σ <sub>a</sub> /barns
Crystal Structure	Hexagonal
Electron Configuration	1s <sup>2</sup> 2s <sup>2</sup> p <sup>6</sup> 3s <sup>2</sup> p <sup>6</sup> d <sup>2</sup> 4s <sup>2</sup>
Electrons per energy level	2,8,10,2
Ionic Radius	0.605Å
Filling Orbital	3d <sup>2</sup>
Number of electrons (with no charge)	22
Number of neutrons (most common/ stable nuclide)	26
Number of protons	22
Oxidation States	4
Valence electrons	3d <sup>2</sup> 4s <sup>2</sup>

**Table 1-2 - Titanium Atomic Structure**

Chemical Properties	
Electrochemical Equivalent	0.4468g/amp-hr
Electron Work Function	4.33eV
Electronegativity	1.54 (Pauling); 1.32 (Allrod Rochow)
Heat of Fusion	15.45kJ/mol
Ionization Potential	First: 6.82 Second: 13.58 Third: 27.491
Valence Electron Potential	-95.2 eV

**Table 1-3 - Titanium Chemical Properties**

Physical Properties	
Atomic Mass Average	47.88
Boiling Point	3560K 3287°C 5949°F
Coefficient of linear thermal expansion	8.35E-6 <b>K-1</b>
Conductivity	Electrical: 0.0234 10 <sup>6</sup> /cm Ω Thermal: 0.219 W/cmK
Density	4.54g/cc @ 300K
Elastic Modulus	Bulk: 108.4/GPa

	Rigidity: 45.6/GPa Youngs: 120.2/GPa
Enthalpy of Atomization	468.6 kJ/mole @ 25°C
Enthalpy of Fusion	15.48 kJ/mole
Enthalpy of Vaporization	429 kJ/mole
Heat of Vaporization	421kJ/mol
Melting Point	1933K 1660°C 3020°F
Molar Volume	10.64 cm <sup>3</sup> /mole
Physical State (at 20°C & 1atm)	Solid
Specific Heat	0.52J/gK
Vapor Pressure	0.49Pa@1660°C

**Table 1-4 - Titanium Physical Properties**

### ***1.2.2. Stability of Molecules***

Substance	$\Delta H^{\circ}$ (kJ/mol)	$S^{\circ}$ (J/Kmol)	$\Delta G^{\circ}$ (kJ/mol)
Titanium Metal (Ti) solid	0	30.29	0
Titanium Carbon (TiC) solid	-226	24.3	-222
Titanium Oxide (TiO) solid	-478.83854	34.77	-489.2
Titanium Dioxide (TiO <sub>2</sub> ) solid	-912.1	50.25	-888.4
Titanium(III) Oxide (Ti <sub>2</sub> O <sub>3</sub> ) solid	-1535.5	78.78	-1432.2
Titanium(V) Oxide (Ti <sub>3</sub> O <sub>5</sub> ) solid	-2443	129.4	-2314
Titanium(II) Hydroxide (Ti(OH) <sub>2</sub> ) solid	Not Available	Not Available	-1058.552
Titanium(III) Hydroxide (Ti(OH) <sub>3</sub> ) solid	Not Available	Not Available	-1049.8
Titanium Chloride (TiCl) gas	439.3	Not Available	Not Available
Titanium Dichloride (TiCl <sub>2</sub> ) solid	-477	108.8	-401.7
Titanium Trichloride (TiCl <sub>3</sub> ) solid	-699.3	127.6	-619.2
Titanium Tetrachloride (TiCl <sub>4</sub> ) liquid	-750.2	252.7	-674.5

**Table 1-5 - Titanium Stability of Molecules [14][15]**

### ***1.2.3. Oxide Layer***

Titanium is known as being corrosion resistant because of the formation of a titanium oxide passivating layer, which is not easily soluble even in acidic media. Studies showed

that the oxide layer is unstable in low levels of pH and high fluorine concentrations, which has even a stronger affinity for titanium atoms than oxygen [16]. The low levels of pH justify the use of very acidic solutions when EP titanium materials. Studies on anodic dissolution of titanium in NaCl-Ethylene Glycol solutions [17] indicate that the titanium oxide layer is unstable using this supporting electrolyte at potentials over 10V.

### **1.3. Conventional Polishing Techniques**

#### ***1.3.1. Abrasive Techniques***

Abrasive polishing is a finishing process for removing asperities using an abrasive work wheel. The wheel is a sanding block, which carries a thin layer of compound, which is the sand paper. The compounds are made from a wax substance which has different abrasive powders added to it. When this hard block is applied to the edge of a spinning buffing wheel, the heat from the friction melts the wax, and both wax and abrasive are applied in a thin slick to the face of the wheel. These methods have disadvantages such as high dishing and erosion. In addition, this technique leaves micro-scratches and cannot polish complex shapes very well [18].

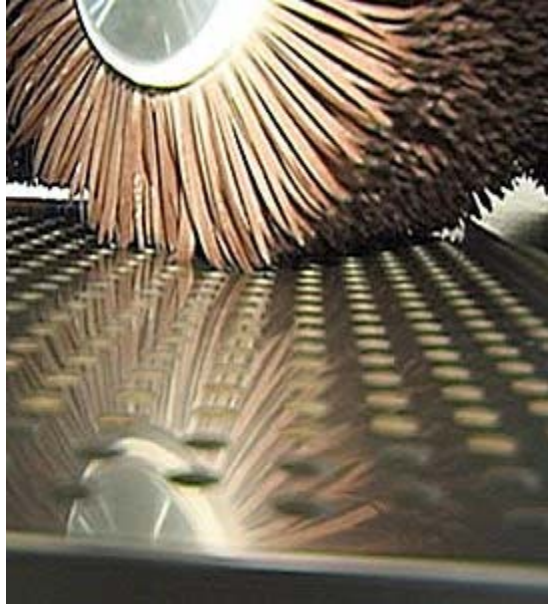


**Figure 1-2 - Abrasive Polishing of a Metal Plate [19].**

### ***1.3.2. Large Area Electron Beam Irradiation***

A magnetic field is generated by a solenoid coil mounted on the outer side of the chamber as shown in Figure 1-3. When the magnetic field is at maximum intensity, pulse voltage is loaded to a ring shape anode. In the chamber, the electrons start to move towards the anode. Simultaneously, the electrons move spirally because of the applied Lorentz forces. Next, argon atoms inside the chamber are ionized by the repetitious collision with electrons, which generates plasma near the anode. When the plasma intensity takes a maximum, pulse voltage is applied to the cathode. The electrons are accelerated by high electric field due to electric double layer formed near the cathode, and the explosive electron emission occurs. Then an electron beam with high energy density is irradiated to the work piece surface and leads to the melting of the metal. The advantages of this technology is that one can achieve very good results and can lower the roughness of a flat

surface to as low as 0.7  $\mu\text{mRz}$  [20]. The disadvantages of this method are that it is expensive and difficult to operate due to its complexity [20].

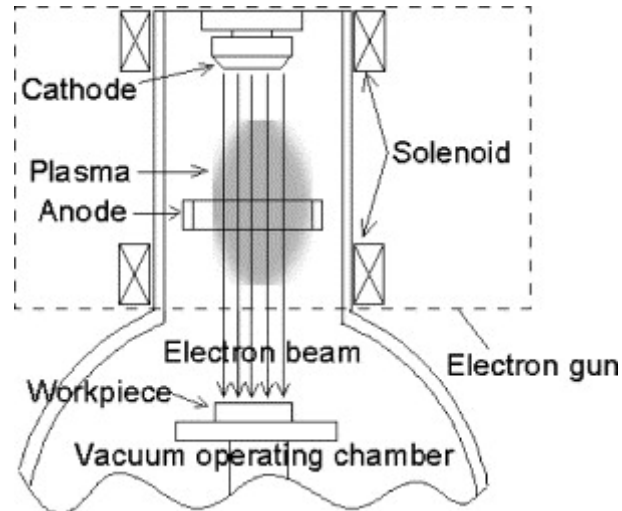
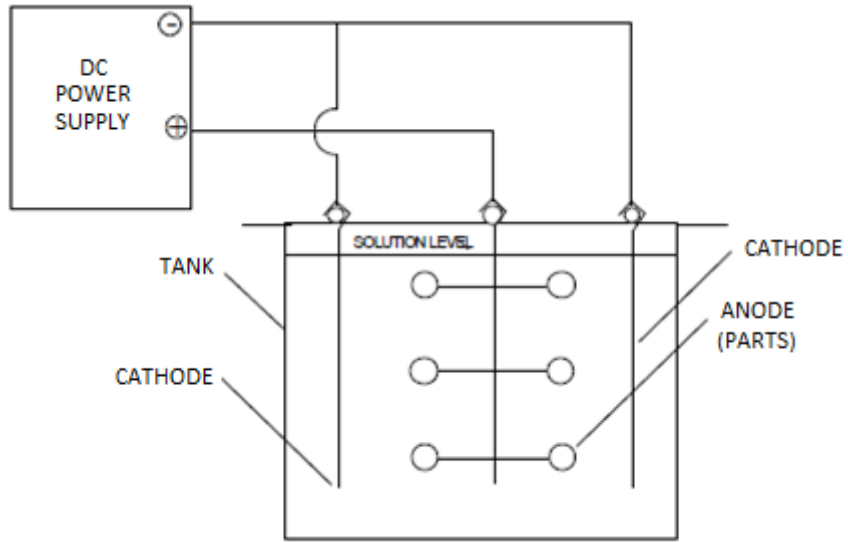


Figure 1-3 - Large Area Electron Beam Irradiation [20].

### ***1.3.3. Electropolishing***

Electropolishing is a process by which metal is removed from a workpiece by passage of electric current while the work piece is submerged in an electrolyte. The process is essentially the reverse of electroplating. In a plating system, metal ions are deposited from the solution onto the work piece; in an electropolishing system, the work piece itself is dissolved, adding metal ions to the solution. This method, very simple and easy to operate, requires a relatively small capital investment. Multiple parts can be polished at the same time and the complexity of the geometry is not a problem since the electrolyte solution submerges the entire part. Figure 1-4 illustrates a typical electropolishing setup. More detail will be given in chapter 2.



**Figure 1-4 - Schematic Illustration of a Typical Electropolishing System.**

## **2. Electropolishing**

This chapter begins by introducing the important fundamentals of EP presented in literature. A general overview of the process is given followed by proposed mass transport mechanisms of the metal ions that are being dissolved from the bulk material into the electrolyte solution. These suggest that the process is limited, not by electron transfer, but by diffusion of the metal ions away from the working electrode surface in the case of our application. The ratio between planar and spherical diffusion is presented analytically and a 2D simulation was developed in this study to verify the evolution of the Nernst diffusion layer for a surface with asperities modeled as triangles. The chapter ends by suggesting that the application of electric pulses as opposed to continuous direct current is more effective and equations are presented to model the dissolution process for this pulse technology.

## 2.1. Theoretical Background

Electropolishing is an old process. It was first patented by the German government in 1912 for the finishing of silver in a cyanide solution [21]. Although experimentation continued, the next significant advance was not made until 1935 when copper was successfully electropolished by Pierre Jacket. During World War II, new developments were achieved [22].

Electropolishing is commonly described as the reverse of electroplating. The working electrode is placed as an anode and cathodes are usually made of an inert material, normally platinum or graphite. When a current is applied, the anode dissolves and the concentration of the metal in the solution increases.

Figure 2-1 shows a typical electropolishing apparatus.

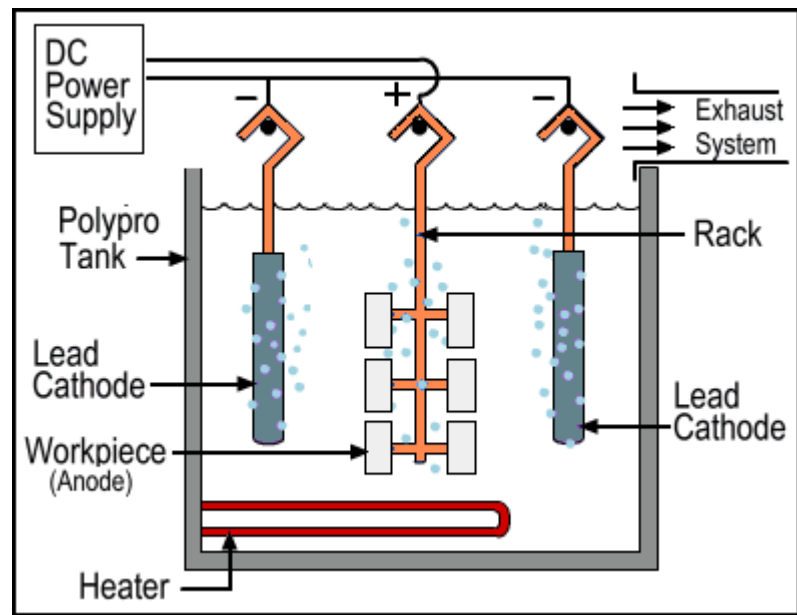


Figure 2-1 - Schematic Illustration of a Typical Electropolishing System.

In the setup of Figure 2-1, the power supply is connected to two cathodes and one anode, on which all the working pieces are attached and they are all placed in an electrolyte. A heating probe is often added to monitor the temperature, an important factor of the process.

Conventionally the process consists of three steps:

1. Metal Preparation
2. Electropolishing
3. Post Treatment

This thesis only focuses on the electropolishing step.

## **2.2. Mass Transport Mechanisms**

Mass transport plays a dominant role in anodic metal dissolution for shaping and surface structuring [23]. Mass transport controlled dissolution results in surface smoothing because peaks of a rough surface diffuse at higher rates than recesses, resulting in surface leveling of the metal. In literature it is common to distinguish anodic leveling or smoothing from anodic brightening. The former refers to the elimination of surface roughness of height  $> 1 \mu\text{m}$  and the later to the elimination of surface roughness comparable to the wave lengths of light [24] resulting in surface brightening [23].

Two transport mechanisms have been proposed for this process: the duplex salt film model and the adsorbate acceptor model [25].

### 2.2.1. The Duplex Salt Film

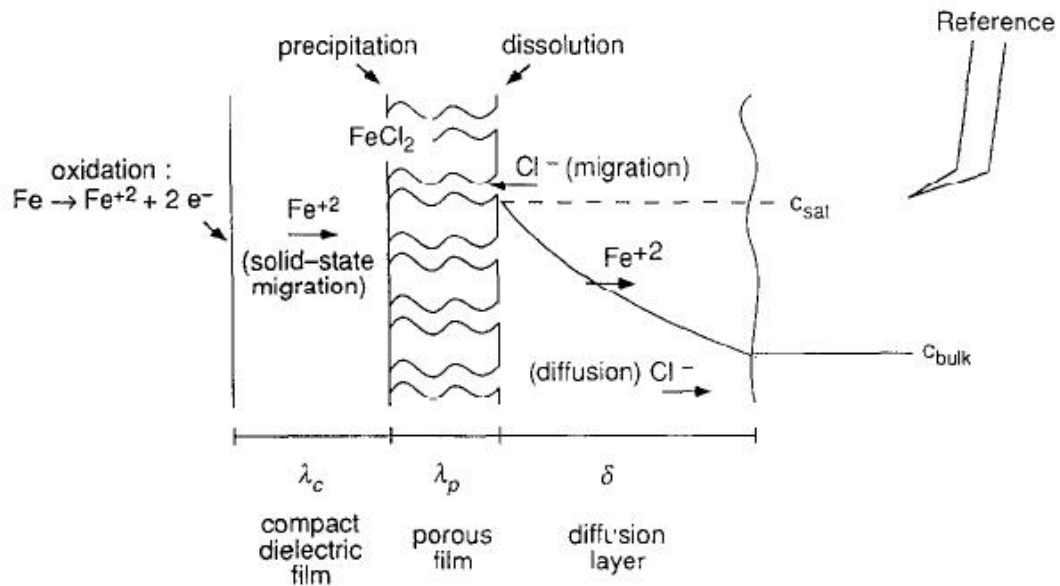


Figure 2-2 - Duplex Salt Film Transport Mechanism [25].

The duplex salt film is shown in Figure 2-2. The rate of transport of dissolving metal ions from the anode surface into the bulk is rate limiting. At the limiting current, a thin salt film is present on the surface and the concentration of dissolving metal ions at the surface corresponds to the saturation concentration of the salt formed with the electrolyte anions.

In this model there are two layers: a compact dielectric film and a porous film. In the compact-film region, the precipitate forms a solid dielectric barrier through which the cations are transported by solid-state ionic conduction in the presence of a much higher electric field. Due to the lower mobility of the ions for solid-state transport, compact films are generally considered to have thicknesses on the order of 10nm, much thinner than the corresponding porous layers.

In the porous-film region, the pores of the precipitate are filled with electrolyte solution and the mobile charge carriers (anions and cations) transport the current by migration in the electric field in the pores [25].

### 2.2.2. Adsorbate Acceptor Model

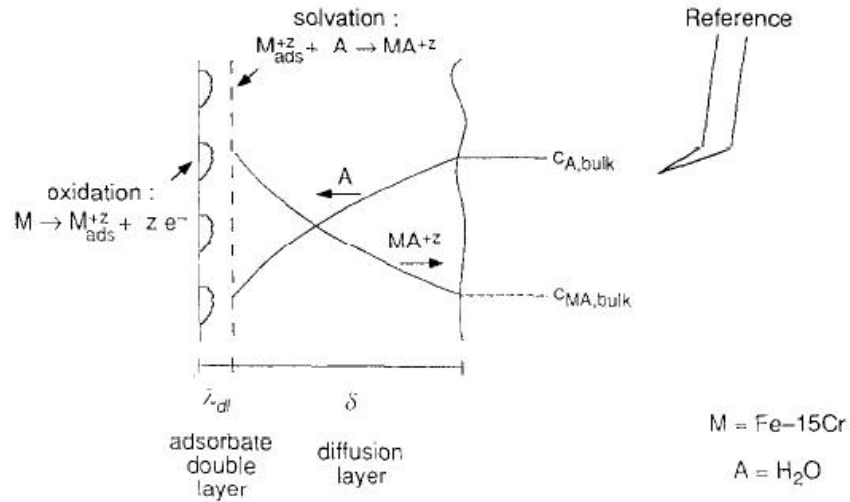


Figure 2-3 - Adsorbate Acceptor Model Transport Mechanism [25].

The adsorbate acceptor model is shown in Figure 2-3. The rate of transport of the acceptor ions such as complexing ions or water towards the anode is the limiting factor. These species react with the dissolving metal ions to form complexed or hydrated species. At the limiting current, the surface concentration of the acceptor is zero and it approaches a constant value the further away from the electrode.

### 2.3. Diffusion and the Nernst Diffusion Layer

As mentioned in the mass transport section, diffusion is an important factor in understanding electropolishing. Therefore a model for diffusion is needed: Fick's First

and Second Laws of Diffusion. Since the reaction is considered to be heterogeneous (reaction occurs at the electrode surface only), an electroactive species being consumed decreases as it approaches the anode and creates a concentration profile with respect to distance. If the concentration becomes zero at the surface, which happens when the electric potential exceeds the current limiting voltage, more electroactive species must diffuse to the electrode in order for the reaction to proceed. This causes an almost linear decrease in the concentration profile of the species.

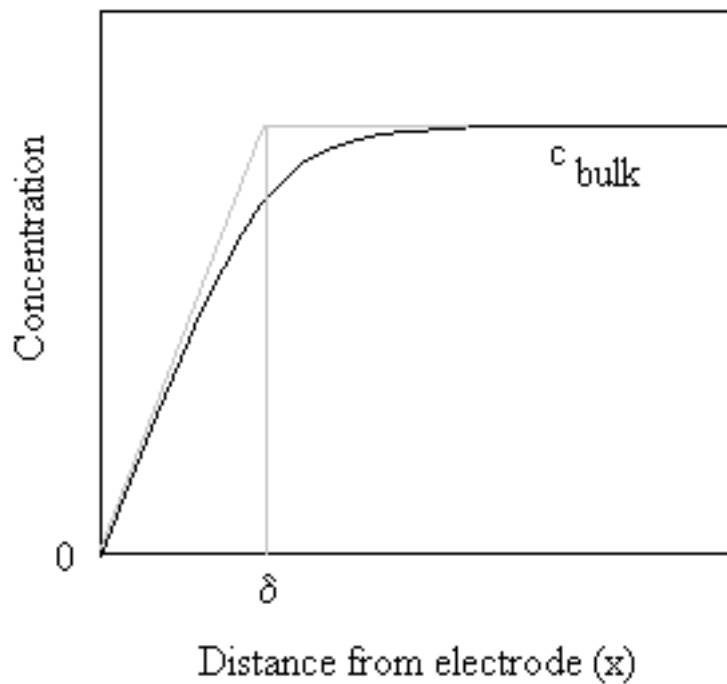


**Figure 2-4 - Depiction of the Nernst Diffusion Layer.**

As can be seen in Figure 2-4, the concentration starts decreasing from its bulk level while it approaches the electrode. The Nernst diffusion layer is defined as the distance at which the bulk concentration line and the derivative of the concentration profile at the surface

meet and is usually represented in literature by the symbol “ $\delta$ ”. It then becomes obvious that at high voltages, the rate of electron transfer at the electrode is much faster than the rate at which the electroactive species reaches the electrode: the process is mass transport controlled under these conditions. Also, at these voltages, the concentration of the electroactive species at the electrode surface is zero for a species that is being consumed.

#### **2.4. Rate of Dissolution and Current Density**

The rate at which the titanium cations are being dissolved is proportional to the electric current. As current density is directly proportional to reaction rate, it is important to be able to model the current density of the work piece. Since the piece is rough, it contains asperities. These can be modeled as being circular: an asperity with a large radius will be relatively flat at its perimeter and approaches linear as the radius “ $r$ ” goes to infinity. An asperity with a small radius will be opposite and therefore deviate from flat. It is then possible to model the current density of a circular asperity compared to a flat surface.

Fick’s first law equates the total flux of material through a cross sectional area due to a concentration gradient varying with the  $x$  axis where  $j$  is the flux ( $\text{mol}\cdot\text{m}^{-2}\cdot\text{s}^{-1}$ ) of a given material,  $D$  is the diffusion coefficient ( $\text{m}^2\cdot\text{s}^{-1}$ ) and  $c$  is the concentration ( $\text{mol}\cdot\text{m}^{-3}$ ). All units are in the international system of units.

$$j = D \frac{\partial c}{\partial x} \quad (2-1)$$

For any species, the equation that models the concentration with time due to diffusion caused by a concentration gradient is Fick’s Second Law.

$$\frac{\partial c}{\partial t} = D \frac{\partial^2 c}{\partial x^2} \quad (2-2)$$

Solving the linear, second order, partial differential equation considering  $D \neq f(c)$  one can obtain equation 2-3 with the following boundary conditions:

- The initial concentration in the electrolyte solution is constant.  $c(x,0) = c_o$

In this application it is 0.

- The surface concentration is fixed during all times.  $c(0,t) = c_s$

This is reasonable considering that the duplex salt film transport mechanism suggests a fixed concentration of the titanium species at the saturation level in the salt layers.

- The concentration at an infinite distance from the electrode is equal to the initial concentration at the bulk during all times  $c(\infty,t) = c_o$

This assumption is reasonable considering the small amount of time in which the voltages are applied and the reasonable size of the cell. As more titanium species gets dissolved into the electrolyte solution, this assumption gets less accurate.

Erf is a standard mathematical function called the error function, tabulated in the book “Handbook of Mathematical Functions” [26].

$$c(x, t) = (c_o - c_s) \operatorname{erf} \left\{ \frac{x}{(\pi Dt)^{0.5}} \right\} \quad (2-3)$$

In this equation,  $c_s$  is the concentration at the surface while  $c_o$  is the concentration in the solution. For small values of  $x \cdot (\pi Dt)^{-0.5}$ , one can simplify equation 2-3 with equation 2-4 with a high degree of accuracy. Since the diffusion is occurring very close to the electrode surface, this assumption is quite reasonable.

$$c(x, t) = (c_o - c_s) \cdot \left\{ \frac{x}{(\pi Dt)^{0.5}} \right\} \quad (2-4)$$

Considering that  $c_s = 0$  (the reaction is being totally controlled by mass transport) and by differentiating at  $x = 0$ , one will have the slope of the concentration profile at the surface of the work electrode at the limiting current. This will lead us to equation 2-5:

$$j_{lim} = c_o \left( \frac{D}{\pi t} \right)^{0.5} \quad (2-5)$$

The same equations can be used to solve the variation of concentration for spherical diffusion where  $erfc$  is the complement of the error function and is simply  $1 - erf\{z\}$ .

$$c(r, t) = c_o \left\{ 1 - r_o/r \cdot erf c \left[ \frac{r - r_o}{(4Dt)^{0.5}} \right] \right\} \quad (2-6)$$

Differentiating at  $r=r_o$  will result in the following equation:

$$j_{lim} = D c_o \left[ \frac{1}{(4Dt)^{0.5}} + \frac{1}{r_o} \right] \quad (2-7)$$

These equations are valid when the boundary conditions mentioned above are satisfied and by neglecting any convection effect. Approximately after 10 seconds of mass transport controlled dissolution, convection plays a key contribution to mass transport and the equations are no longer precise.

Equating the ratio between spherical (2-5) and planar (2-7) diffusion one can obtain equation 2-8:

$$\frac{j_{lim\ sph}}{j_{lim\ pla}} = 1 + \left[ \frac{(\pi Dt)^{0.5}}{r_o} \right] \quad (2-8)$$

This leads to a few conclusions:

- The ratio between spherical and planar is 1 when  $t=0$ , which makes sense since there needs to be time for the concentration profiles to evolve.
- As  $r_0$  goes to infinity, the ratio approximates 1 which makes sense since for a fixed distance of the perimeter of the sphere, the surface will tend to be more planar as  $r_0$  gets larger.

The current density ratio versus the asperity size over time can be plotted, as seen in Figure 2-5. The plot was done considering a diffusion coefficient of  $1 \times 10^{-9} \text{ m}^2 \text{ s}^{-1}$ .

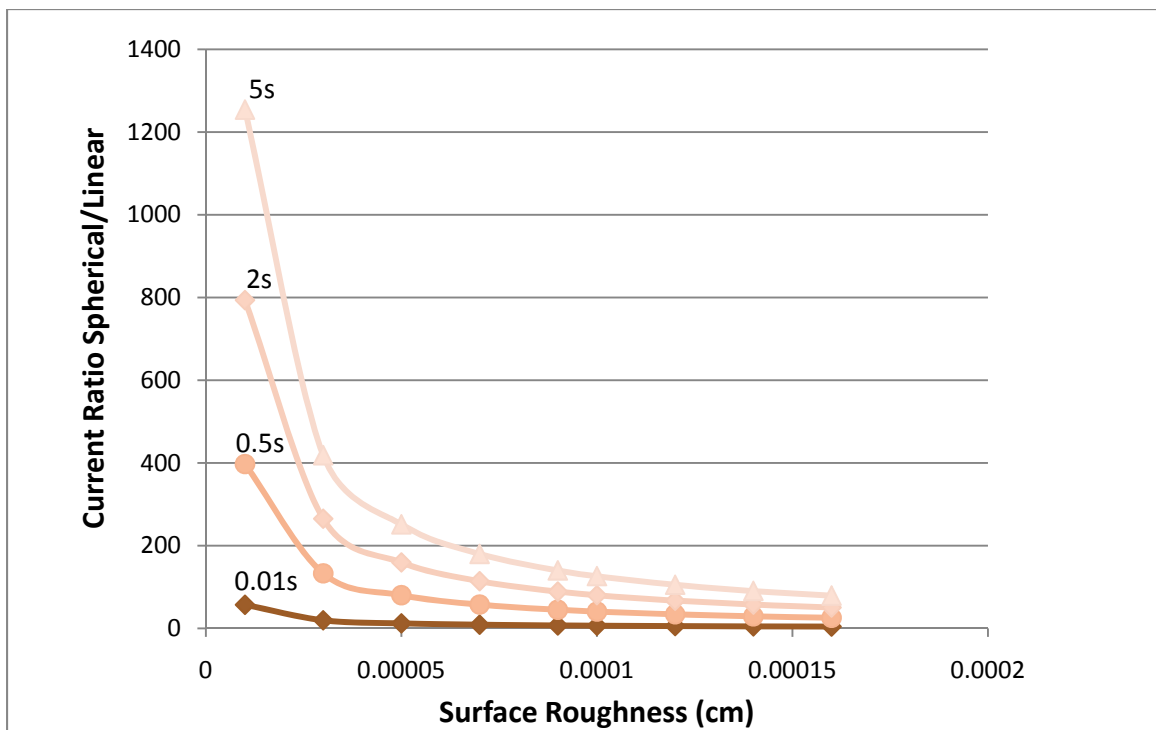
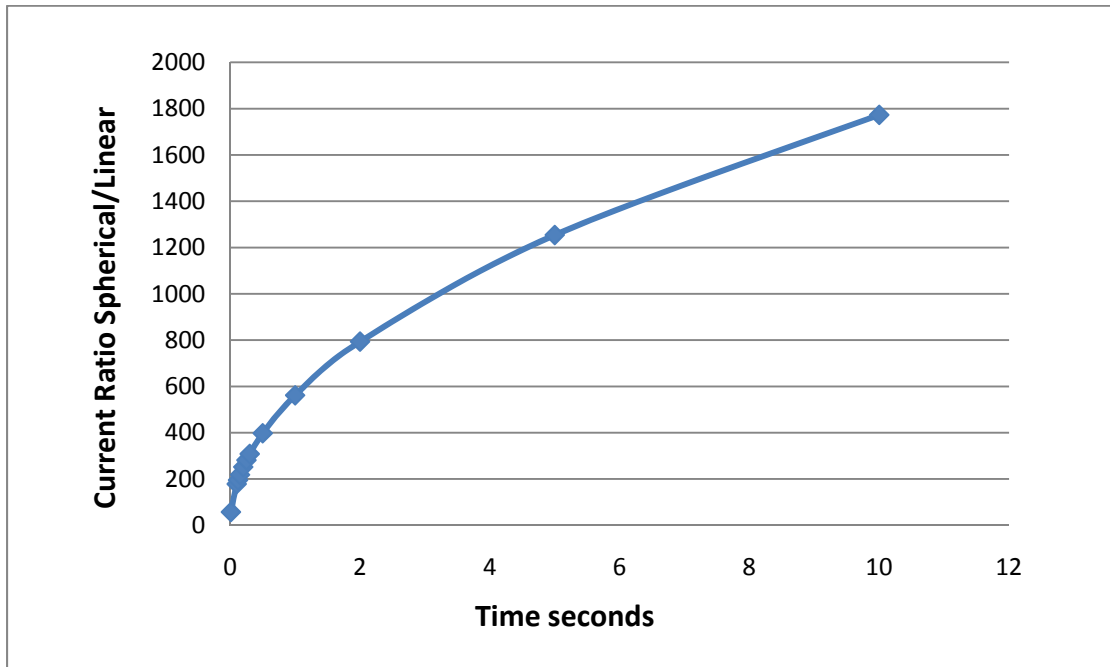


Figure 2-5 - Current Density Ratio x Asperity Size at Different Times.

Figure 2-5 allows us to conclude two important properties. The first is the current density dependence on time. The longer the experiment goes, the larger will be the ratio for a given asperity size. The second conclusion is that as the asperity gets more plane

(increase in radius), the difference in current gets smaller as one would expect from the conclusions drawn above.

Figure 2-6 shows the evolution between the ratio of spherical and planar diffusion with time for a certain asperity size. The size chosen for the plot was  $1\mu\text{m}$ .



**Figure 2-6 - Time Evolution of Ratio Between Spherical and Linear Diffusion.**

From these analyses, one can conclude that the longer the time the greater the difference between spherical and linear diffusion leading to surface smoothing. However, this analysis was done considering two isolated systems. Since the asperities are close together with the planar surfaces, the concentrations profiles overlap and as the Nernst diffusion layer gets bigger, it tends to make the system less efficient as will be discussed further.

## 2.5. Characterization of the Nernst Diffusion Layer Evolution

The Nernst Diffusion layer is characterized by the extent in which the concentration profile of an electroactive species extends from the electrode to the bulk solution. Since the process is governed by mass transport, the rate of dissolution can be modeled by Fick's First Law of Diffusion as demonstrated above.

Since the flux is proportional to the concentration gradient, the larger the gradient, the more intense the rate of the reaction will be, in this case, the dissolution of the titanium species.



A 2D simulation of the evolution of the Nernst diffusion layer has been made using the software Comsol Mutiphysics version 3.5a. An arbitrary work piece with two sizes of asperities modeled as triangles was designed. The concentration of the Ti ions was fixed at the surface as proposed by the duplex salt film layer transport mechanism [25]. The concentration chosen was  $1000 \text{ mol.m}^{-3}$ . The chosen diffusion coefficient was  $5 \times 10^{-9} \text{ m}^2 \text{ s}^{-1}$  and different quantities of mesh elements were tested and no differences in results were noticed. The pictures below were taken from a simulation running 745 mesh elements. The evolution of the concentration profiles can be separated in 3 different stages.

In the first stage, the Nernst diffusion layer contours both sizes of asperities of the work piece as shown in Figure 2-7.

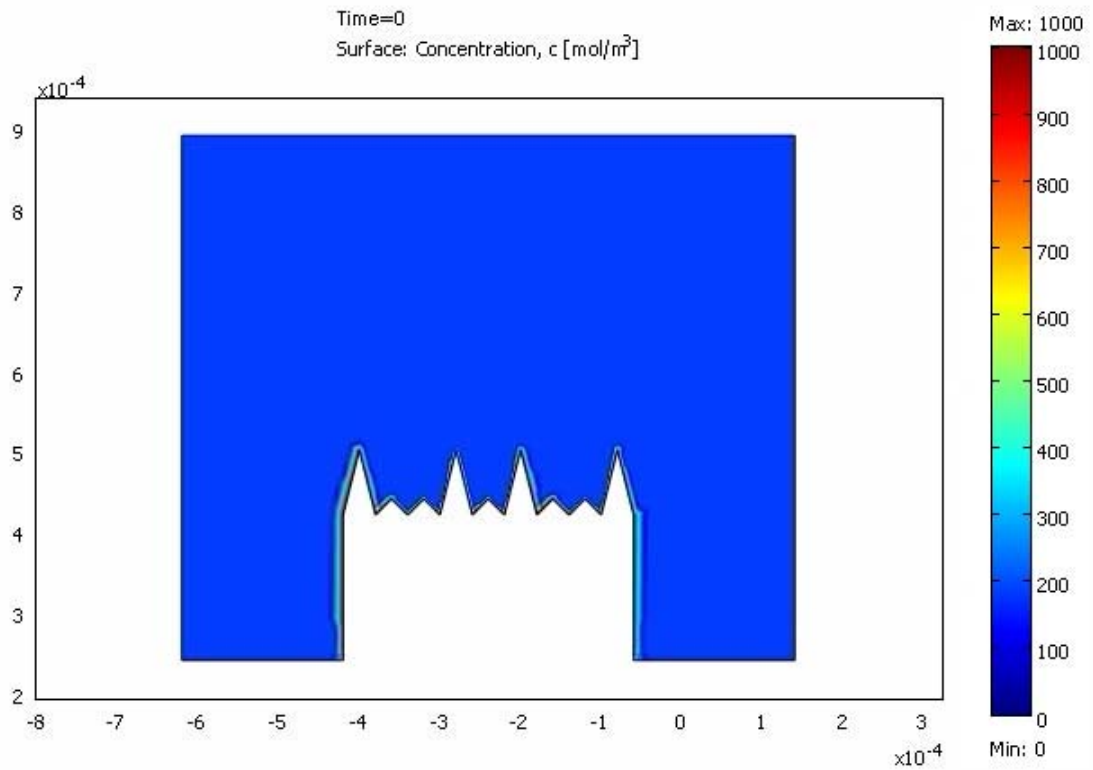


**Figure 2-7 - First Stage: Nernst Diffusion Layer Evolution with Time.**

Since the concentration gradient is very large throughout the entire surface area in this stage, it is characterized by an intense rate of dissolution.

The second stage is characterized by the development of the layer to a point where it no longer contours the smaller asperities, but still contours effectively the large ones. In this case, the dissolution will be higher on the larger asperities tending to make them smaller, approaching the size of the smaller ones.

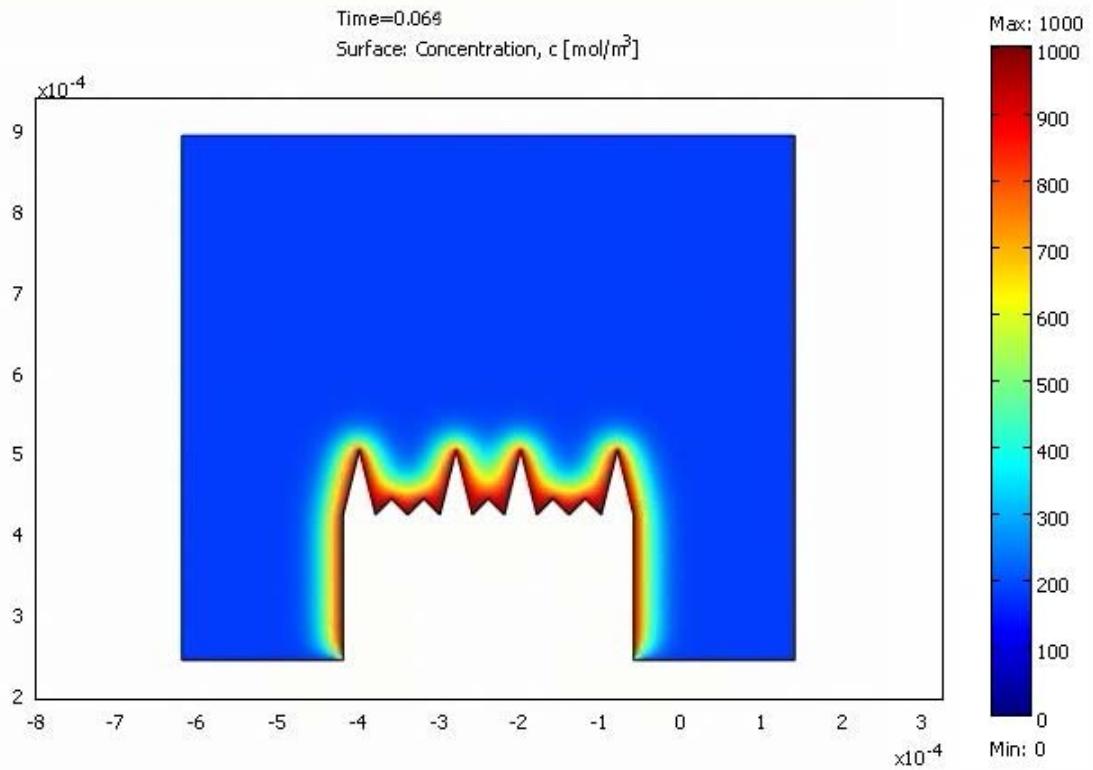


**Figure 2-8 - Second Stage: Nernst Diffusion Layer Evolution with Time.**

In the third stage, the Nernst diffusion layer no longer contours any of the asperities of the work piece. In this case, the rate of dissolution is not as high as the previous stages and there is not much of a difference in gradient between larger asperities and smaller ones.

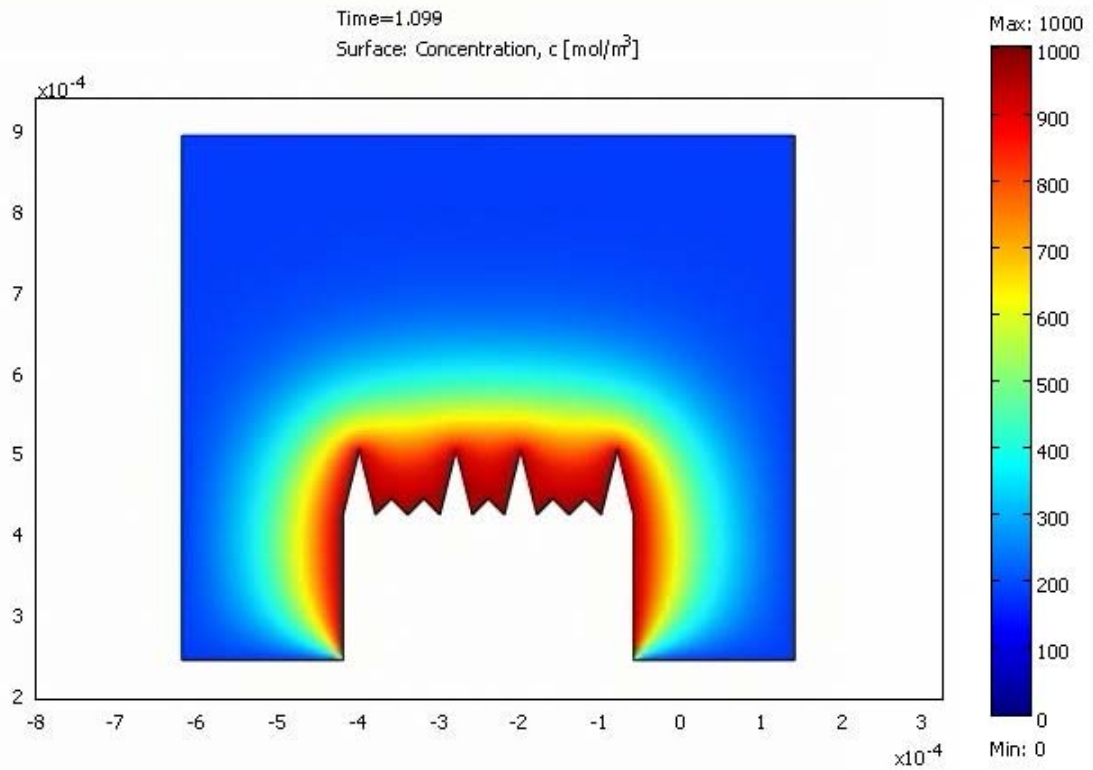


**Figure 2-9 - Third Stage: Nernst Diffusion Layer Evolution with Time.**

One can conclude from this simulation that the more time is spent on stage 2 the better since higher asperities will dissolve more than lower ones and to planar surfaces resulting in a net smoothening of the surface. However, one cannot reach stage 2 without passing through stage 1. Ideally, one should pass through stage 1, reach stage 2 and, while approaching stage 3 one should stop the applied electric voltage in order to “reset” the diffusion layer.

The ideal periods of time of each stage depends on the diffusion coefficient and the roughness profile of the workpiece (dimensions and ratio between the larger and smaller asperities). It is self evident that with the dynamic change in the roughness profile with

the dissolution, there will be different ideal voltage pulse widths throughout the polishing process. A way of sensing this change could be perhaps with the total current, since the total current will change since the total surface area exposed to the electrolyte tends to decrease while the process takes place. A relation between the current and the roughness profile is an interesting topic for investigation which could lead to a dynamic algorithm to control the duration of the electric pulse.

## 2.6. Limitations of Traditional EP

Traditional EP uses direct current and therefore it is not able to enhance the ratio of the asperity versus planar dissolution. Therefore extensive amounts of material need to be dissolved in order to produce reasonable results.

Several companies advertise up to a possible 50% reduction in the surface roughness profilometer readings of a part by EP. For example, an initial surface roughness of 30Ra can be lowered down to 15Ra. If a 50% reduction does not fulfill the necessary requirements, then they recommend other polishing methods, most times mechanical, prior to EP. Table 2-1 has examples of companies that follow this guideline.

Company Name	Uniform Resource Locator	Advertised Roughness Improvement	Main Advertised Materials
Able Elect.	<a href="http://www.ableelectropolishing.com">www.ableelectropolishing.com</a>	Reduction of up to 50%	Steel, Stainless Steel, Aluminum, Copper, Nickel, Titanium
MCP Elect.	<a href="http://www.electropolish.com">www.electropolish.com</a>	Reduction of up to 50%	Steel, Stainless Steel, Copper
Kalamazoo Elect.	<a href="http://www.kepcoinc.com">www.kepcoinc.com</a>	Reduction of up to 50%	Steel, Stainless Steel, Copper
New England Elect.	<a href="http://www.nееlectropolishing.com">www.nееlectropolishing.com</a>	Reduction of up to 50%	Stainless Steel, Nickel, Tungsten, Molybdenum

Delstar Metal Finishing	<a href="http://www.delstar.com">www.delstar.com</a>	Reduction of up to 50%	Steel, Stainless Steel, Aluminium, Copper, Titanium, Bronze, Nickel, Silver, Gold
Harrison Elect.	<a href="http://www.harrisonep.com">www.harrisonep.com</a>	Reduction of up to 50% (usually between 10-35%)	Stainless Steel, Nickel,

**Table 2-1 - Electropolishing Companies**

Satisfactory results with titanium are even more difficult. Until the present day, good results have not yet been achieved in industry according to several companies. This led DynaTools to invest on research and development although they had never done EP before.

Another reason for limitations in electropolishing Ti in industry today is the electrolyte used. Even though they are very acidic, the surface normally passivates to some degree due to the high affinity of titanium with the oxygen atom, which limits the amount of time the parts can be exposed to EP.

## **2.7. Modeling Mechanism for the Pulse Technology**

The process is initiated by an applied voltage which results in dissolution of the Ti species. As the Ti species reacts with the chloride anions, the duplex salt layer film starts building until its full development. After this happens, the process becomes limited by mass transport. The process can be modelled by the following steps:

- 1) In the initial stage, since there is no salt film to limit the reaction rate by mass transport, the electron transfer rate prevails in the anode side and the surface area of the cathode is what limits the reaction. If there would be sufficient surface area

in the cathode, than this stage could be modeled using the Butler Voltmer equation (2-10):

$$j_{total} = j_o \left[ \exp\left(\frac{(1 - \alpha)nF(E - E_{rev})}{RT}\right) - \exp\left(\frac{-\alpha nF(E - E_{rev})}{RT}\right) \right] \quad (2-10)$$

In this equation,  $j_o$  is the current density ( $\text{Am}^{-2}$ ),  $n$  is the number of electrons involved in the electrode reaction,  $F$  is the Faraday constant,  $E$  is the electrode potential (V),  $E_{rev}$  is the equilibrium potential (V),  $R$  is the universal gas constant and  $\alpha$  is the symmetry factor.

Since high over potentials are applied in the process, one of the half reactions becomes dominant and the equation can be simplified with a high degree of accuracy to equation 2-11:

$$j_{total} = j_o \left[ \exp\left(\frac{(1 - \alpha)nF(E - E_{rev})}{RT}\right) \right] \quad (2-11)$$

Since the over-potentials applied in the present work are normally around 30V, the values from this equation are very high. For example, considering a symmetry factor  $\alpha$  of 0.5 and the number of electrons  $n$  as 1 (4 times less than the suggestive valence of Ti being dissolved), the value being inputted into the exponential function is around 580. This leads to a very high number, which would be limited by the reaction rate at the cathode electrode or by some other factor. Therefore, ideally the larger the surface area in the cathode the better. Experimentally, cathode surface areas around 30 times greater than anode have given satisfactory results.

Since the first stage of the process, which involves the development of the duplex salt layer film is not governed by mass transport, this stage does not effectively improve surface finishing and the design of the pulse width should take this into consideration.

Considering that the anodic reaction of equation 2-9 occurs at the current efficiency of 100% and valence of 4, the amount of titanium cations dissolved into the electrolyte can be modeled using Faraday's equation that relates the current with the amount of atoms participating in the reaction:

$$N = \frac{It}{nF} \quad (2-12)$$

In this equation, N is the amount of product (mol), I is the current (amp), t is the time (s), *n* is the number of electrons and F is the Faraday constant. With the dissolution of titanium species, the titanium ions are attracted to the chloride anions by the columbic forces. After reaching the saturation point, these molecules start precipitating and a layer starts building. The layer will keep on growing until the potential drop limits the electric potential gradient in the solution near the electrode and the dissolution of titanium species becomes controlled by diffusion. If a higher potential is applied, the salt layer film thickness will increase until the solution near the outer film has an electric potential gradient of nearly 0.

The higher the electric potential, the higher the current and thus greater will be the reaction rate and more intensely the salt layer film will start developing. However, the higher the electric potential, the thicker the film will be once steady state is reached.

2) The thickness of the duplex salt film is a function of the applied over potential. After it is completely developed, the process is then governed by mass transport. During this phase, the reaction can be modelled considering pure diffusion limited dissolution. How quick the titanium ions can diffuse away from the anode is what limits the reaction. Natural convection caused by concentration differences was neglected in this model. The equation below models a pure diffusion limited electrochemical process.

$$j = \frac{nFc \left(\frac{D}{\pi}\right)^{0.5}}{t^{0.5}} \quad (2-13)$$

In this equation,  $j$  is equal to the flux ( $\text{mol}\cdot\text{m}^{-3}\cdot\text{s}^{-1}$ ),  $n$  is the number of electrons,  $F$  is the Faraday constant,  $D$  is the diffusion coefficient ( $\text{m}^2\cdot\text{s}^{-1}$ ),  $c$  is the concentration of the species (mol) and  $t$  is time (s). The size of the pulse should also consider the height of the asperities. For more effective levelling, the size of the Nernst diffusion layer should be less than the size of the larger asperities of the working electrode as shown in the simulation.

3) The lower potential of the pulse gives time to decrease the concentration of cations near the surface decreasing the Nernst Diffusion Layer. This is desired since a large Nernst diffusion layer (bigger than the larger asperities of the work piece) are not as effective as demonstrated in the simulation. If sufficient time is given, the concentration profile will completely level throughout the solution.

The state of the process in any given time (except for the very beginning in stage 1) is most likely to be a transition of the steps above. While working with pulses in the microsecond range, most likely the salt film does not have time to dissolve itself and the process is probably taking place in steps 2 and 3.

### **3. The use of Ethylene Glycol in Electropolishing of Titanium Materials**

This chapter provides a literature review on the use of ethylene glycol based electrolytes for the electropolishing of titanium materials. Published results illustrate the great potential of this product. Possible reactions taking place have been proposed. Additional experiments, when needed, were conducted to complete available results from the literature.

### 3.1. Ethylene Glycol

Ethylene Glycol is an organic compound composed of two hydroxyl radicals on adjacent carbon atoms (Figure 3-1).

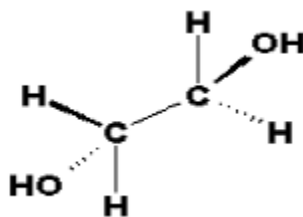


Figure 3-1 - Ethylene Glycol Molecule.

It is widely used in airports along with propylene glycol as aircraft deicing fluids. Another important application is thermal fluid for refrigeration systems since it lowers the freezing point and raises the boiling point of water, enhancing the range of temperatures at which the solution can apply.

The use of ethylene glycol as a less toxic option for EP of titanium was first introduced by Deguchi in 2003[27]. Further studies have been made [17][28], suggesting the development of a thin  $\text{TiCl}_4$  layer when using NaCl which would limit the dissolution rate of titanium by mass transport. The experiments suggest the formation of a duplex salt layer film [25] as described in the previous chapter.

### 3.2. Electrochemical Behaviour of Ethylene Glycol

The electrochemical behaviour of the solvent ethylene glycol was investigated by F. Bonet [29]. Figure 3-2 shows a room temperature voltammogram of ethylene glycol-potassium nitrate solutions recorded using a carbon rotating disk electrode. In this current

density versus potential curve, one can locate the cathodic and anodic potentials corresponding to the reduction and oxidation of ethylene glycol respectively. Potassium Nitrate was chosen as the supporting electrolyte since it is chemically inert towards the components of the system.

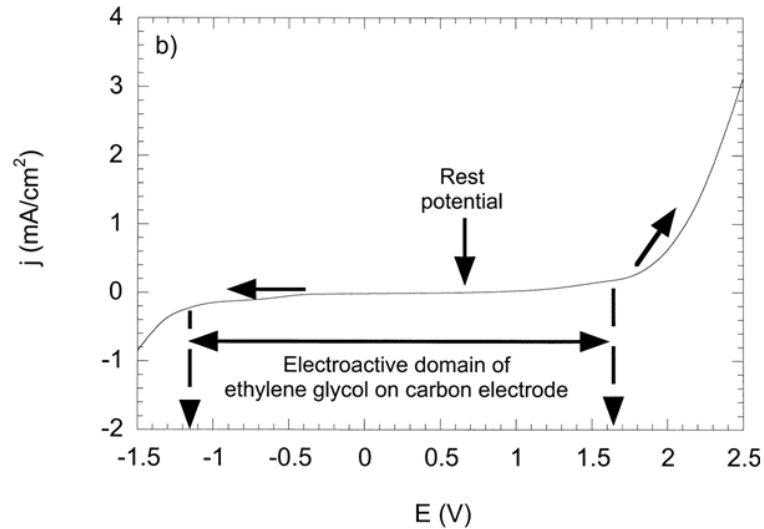


Figure 3-2 - Voltammogram of the Electrochemical Behaviour of Ethylene Glycol [29].

From Figure 3-2, one determines that ethylene glycol starts reducing at a potential of -1.15V (vs SCE) and oxidizing at 1.65V (vs SCE). The products resulting from these have yet to be determined.

### 3.3. Possible Reactions in the Process

#### 3.3.1. Substances Involved

Titanium is the substance to be polished. For counter electrodes, most experiments are being done using carbon or platinum. Both are considered to be inert, not participating in

the reaction. Ethylene Glycol is the solvent. Sodium Chloride (NaCl) is the salt added for conductivity.

### 3.3.2. Dissolution of the Electrolyte

The crystal NaCl is bounded by columbic forces of oppositely charged ions according to equation 3-1.

$$U = \frac{q_1 * q_2}{4\pi * \epsilon_r * \epsilon_o} \quad (3-1)$$

In this equation, q is equal to the charge (C) of the species,  $\epsilon_r$  is the relative permittivity of the medium, and  $\epsilon_o$  is the permittivity of free space ( $F.cm^{-3}$ ) and r is the distance between ions (m). In aqueous solutions, the dissolution process is done due to the increase in relative permittivity of the medium  $\epsilon_r$  ( $\approx 80$  in case of water at room temperature) and also due to the dipole character of water molecules ( $6.7 \times 10^{-30}$  to  $10.0 \times 10^{-30}$  C.m). In ethylene glycol, the relative permittivity is around 37 and the dipole moment is around  $6.7 \times 10^{-30}$  C.m. These values are lower than water, resulting in a less intense dissolution process compared to water solutions. This justifies the fact that it takes less time for the NaCl to dissolve in water than in ethylene glycol while using a shaker.

### 3.3.3. Thermodynamic Data

Table 3-1 lists thermodynamic data of reactants and possible products of the process.

Substance	$\Delta H^\circ$ (kJ/mol)	$S^\circ$ (J/Kmol)	$\Delta G^\circ$ (kJ/mol)
Ethylene Glycol (HOCH <sub>2</sub> CH <sub>2</sub> OH)	-460	166.9	-509.7362
Ethanol (C <sub>2</sub> H <sub>5</sub> OH)	-277.38	159.9	-325.0302
Ethylene Oxide (C <sub>2</sub> H <sub>4</sub> O)	-52.6	243	-125.014
Water (H <sub>2</sub> O)	-285.25	70.12	-306.14576

Titanium Tetrachloride (TiCl <sub>4</sub> )	-750.2	252.7	-825.5046
Titanium Dioxide (TiO <sub>2</sub> )	-912.1	50.25	-927.0745
Titanium Carbon (TiC)	-226	24.3	-233.2414
Graphite (C)	0	5.69	-1.69562
Chloride Ions Aqueous (Cl <sup>-</sup> )	-167.54	55.13	-183.96874
Chloride Gas (Cl <sub>2</sub> )	0	223.09	-66.48082
Hydrogen Gas (H <sub>2</sub> )	0	130.74	-38.96052
Oxygen Gas (O <sub>2</sub> )	0	205.25	-61.1645

**Table 3-1 - Titanium EP with Ethylene Glycol – Thermodynamic Data of Molecules [30][14][15]**

### 3.3.4. Anode: Possible Reactions

In the initial stage of the process, an oxide layer is present in the titanium work piece. This oxide layer is unstable at voltages higher than 10V (Ag/AgCl) [17]. While working with pulses, an increase in the oxide layer can happen depending on the duty cycle. During the high level period of the electric pulse, the most probable reaction is the oxidation of the oxide layer to form oxygen gas [31]. This explains the bubbling in the anode in the beginning of the process when direct current is used.



In order to check realistically if there is enough volume and charge transfer for the oxygen to form bubbles, the following calculations were made. Considering the ideal gas law, the amount of moles of oxygen needed to produce 10 bubbles of a volume of a cube of 3mm side considering a pressure of 3 atmospheres is roughly  $3.29 \times 10^{-5}$  moles ( $3.29 \times 10^{-6}$  per bubble). Titanium dioxide has a density of  $4.23 \text{g.cm}^{-3}$  and a molar mass of roughly  $80 \text{g.mol}^{-1}$ . Therefore, the quantity of moles per  $\text{cm}^3$  is 0.05. Considering a surface area  $1 \text{cm}^2$ , the thickness of the reacted oxide layer according to equation 3-2 would be  $6.6 \times 10^{-6} \text{m}$  or  $6.6 \mu\text{m}$ . Since bubbles are only visualized in the first 300 seconds,

we can also equate the current necessary according to Faraday's law to produce the bubbles. In this case, the current necessary would only be 50mA. These values give very rough estimates and the thickness of the oxide layer can be much thinner considering that the electrochemical active surface area is much larger and that the surface of our work pieces are larger than  $1 \text{ cm}^2$ . Moreover, pressure can easily be much lower than the 3 atmospheres considered. We can conclude that equation 3-2 still remains a possibility.

Figure 3-3 shows gas production at the anode in the initial stage of the process. The gas being produced could be oxygen being generated according to reaction 3-2. After a few minutes, the gas production ceases to be visible and the most likely main electrochemical reaction is the dissolution of titanium. Gas production at the cathode is more intense at all times.

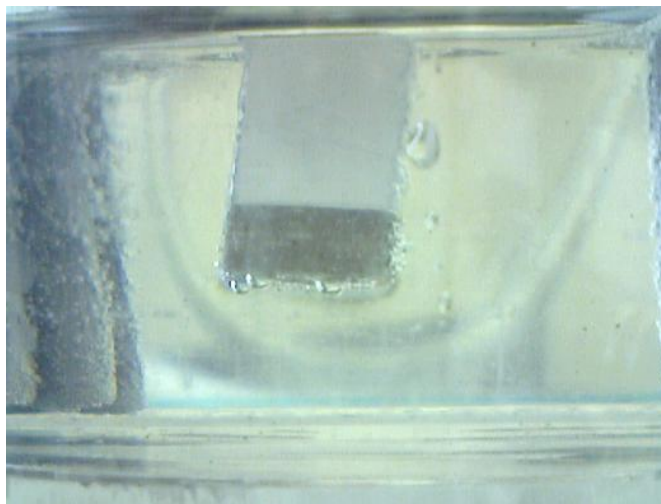


**Figure 3-3 - Ti Being Electropolished. Gas Evolution Occurring in Counter and Working Electrodes.**

Another possibility is the oxidation of the oxide layer and its removal from the surface according to reaction 3-3.



While the pulse is at low level, electron transfer decreases significantly and titanium most likely reacts with the oxygen dissolved in the electrolyte and builds the oxide layer:



Whether an increase in the oxide layer or an effective polish occurs at the end of the process depends highly on the duty cycle. Figure 3-4 shows two titanium pieces that had their lower parts polished and their upper parts were not exposed to the electrolyte solution. The first by a 15% duty cycle and the second by 100% duty cycle (direct current). As can be seen from Figure 3-4, polishing did not occur in the first as opposed to the second.



**Figure 3-4 - Comparison Between Polishing Results with a Low Duty Cycle (left) and a High Duty Cycle (right).**

The use of electric pulses presents good results with very low duty cycles in an oxygen free environment that can be created with an inert gas injection. This present work conducted several experiments confirming this fact. Figure 3-5 show two pieces being polished for 4 hours with a 15% duty cycle with a pulse width of 200 $\mu$ s. The upper

surface of each work piece was not exposed to the polishing, only the lower part. The only main difference between both the processes of polishing was the level of oxygen. The first had a percent oxygen level inside the electrochemical cell of around 20%, as opposed to 0.7% of the second. Both oxygen levels were measured using the oxygen sensor mentioned in the appendix.

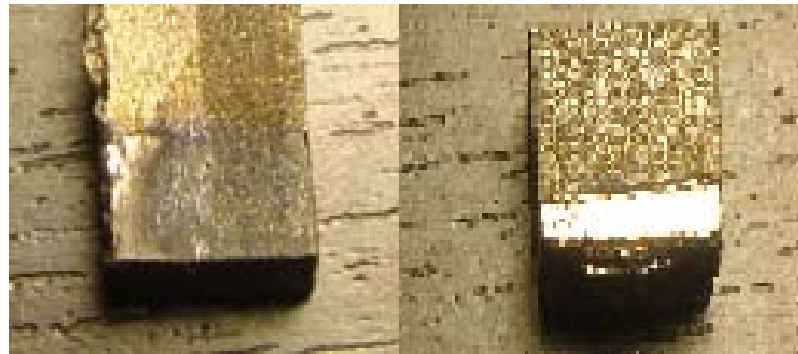


**Figure 3-5 - Comparison Between Polishing Results with Low Duty Cycles, and a High Oxygen Level (left) and a Low Oxygen Level (right).**

After the oxide layer has been removed, the dissolution of titanium takes place. Results showing a decrease in weight of the work piece indicate that titanium atoms are being detached from the bulk material.



Figure 3-6 illustrates a titanium piece polished which significant volume loss can be noticed.



**Figure 3-6 - Titanium Piece with Tip Electropolished.**

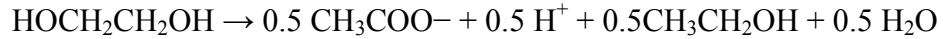
The titanium cations most likely react with the chloride anions to form titanium tetrachloride as proposed by Fushimi [17][28].

### ***3.3.5. Cathode: Possible Reactions***

One of the possibilities of reactions happening on the cathode would be the deposition of sodium cations. But since graphite is normally inert and there is intense gas production, this possibility has been discarded. The most likely reaction taking place is involving the decomposition and reduction of ethylene glycol.

Studies on the electrochemical behaviour of ethylene glycol mentioned above show that the substance starts reducing at a potential of -1.15V(vs SCE) [29].

Since there is a large amount of gas production, the most likely product being generated is hydrogen gas. The only molecule containing the hydrogen atom is ethylene glycol. Here are some possible reactions involving ethylene glycol to produce hydrogen gas [32]:



$$(\Delta G = -21.7\text{kcal})$$



$$(\Delta G = -20.6 \text{ kcal})$$

The electrons being consumed in the cathode region most likely react with  $\text{H}^+$  ions to produce hydrogen gas.

### **3.4. Determination of the Dissociation Valence of Titanium**

The dissociation valence of titanium in ethylene glycol was estimated by Fushimi et al. [17] by applying a constant electric potential of 15V and associating the mass loss with the total amount of charge. A 100% reaction efficiency was assumed or, in other words, the anodic dissolution of titanium contributed to all the current [17]. The authors estimated that the valence of the titanium cations dissolved by the reaction was 4, explaining that the large amount of current in the beginning of the process was due to reactions involving the oxide layer. Figure 3-7 shows the plot obtained.

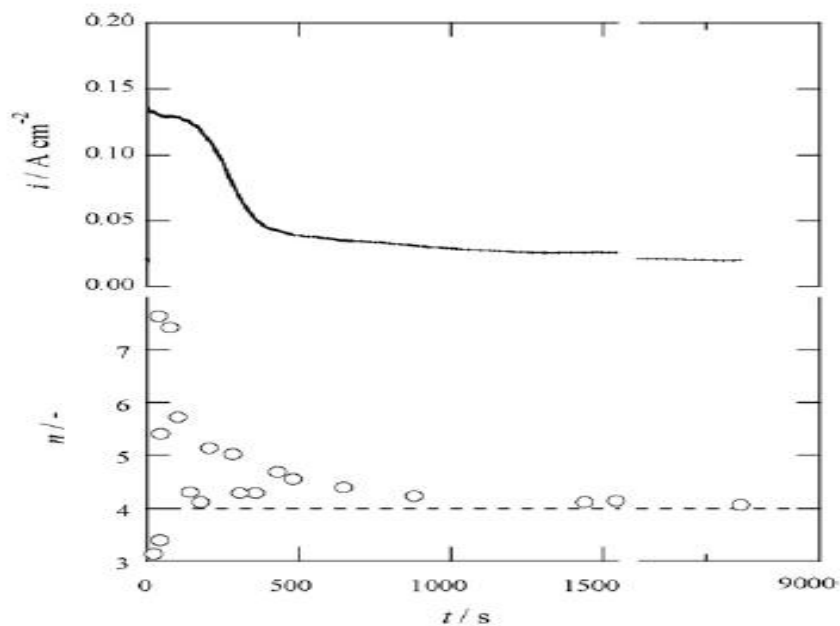


**Figure 3-7 - Current Transient during Anodic Polarization of Ti at 15V in 1M Ethylene Glycol Solution [17].**

### **3.5. Rotating Disk Electrode Experiments**

Following are some current versus potential plots obtained during this research by varying the rotation speed of the working electrode. The voltage was increased at a rate of  $10\text{mVs}^{-1}$ . The electrolyte solution used was 1M NaCl ethylene glycol and graphite rods were used as counter electrodes. One can see on Figure 3-8 that the plateaus established at potentials normally higher than 5V meaning that the reaction is under mass transport control while applying these voltages.

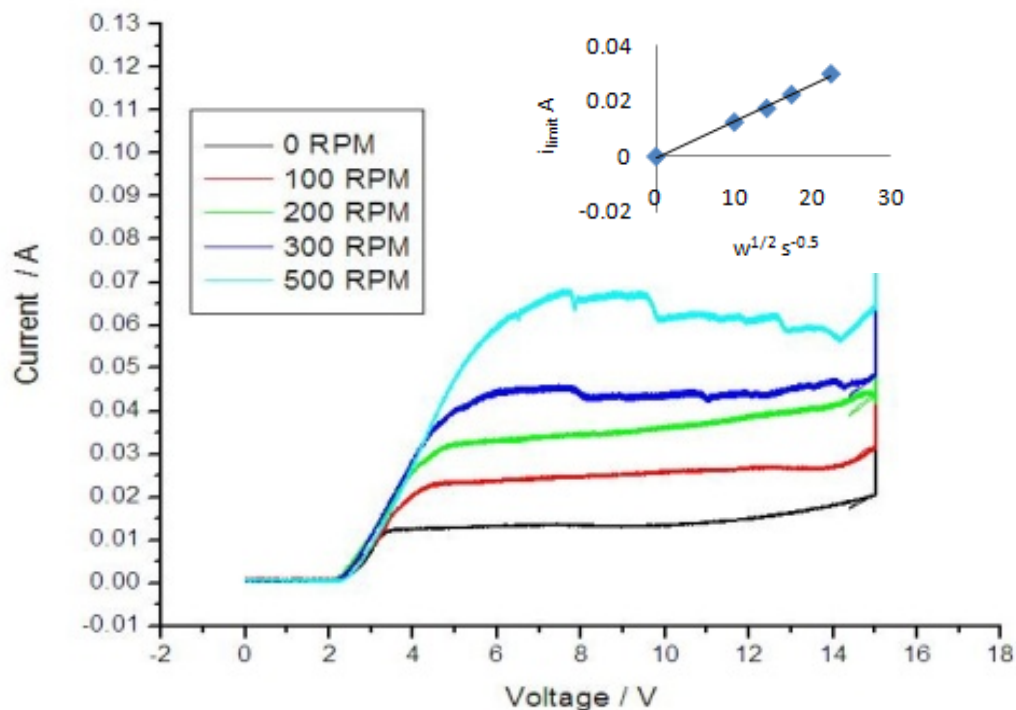


**Figure 3-8 - Anodic Polarization Curves Using a Ti Rotating Disk.**

The results obtained in the present work can be fitted into a Levich plot, as shown in the insert of Figure 3-8, confirming results obtained by Fushimi et al. [17][28]. Since the plotted line passes through the origin, it is possible to confirm that the process is under mass transport control.

### **3.6. Variation with Temperature**

Figure 3-9 shows a plot of current versus temperature for the process obtained in this research. The temperature of the cell was increased and immediately decreased by removing first and placing back the air cooling system. A significant increase in current with the increase in temperature is evident. The lag in response of the temperature sensor

was most likely the reason why the curve generated by decreasing the temperature didn't follow the same path as the one generated by increasing the temperature.

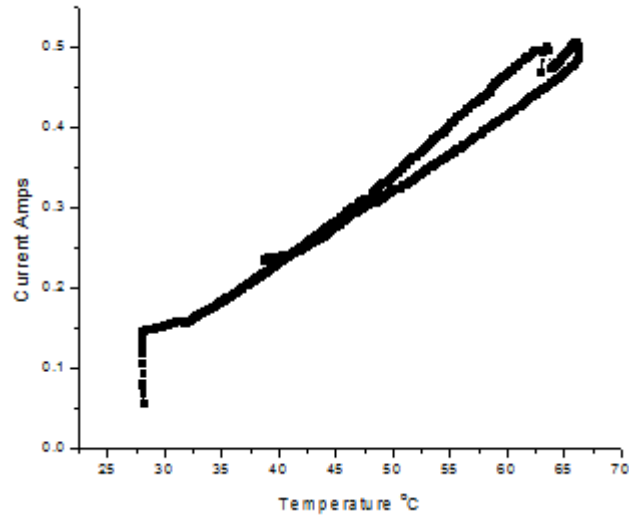


**Figure 3-9 - Current x Temp. Plot of Ti Electropolishing at 15V**

The diffusion coefficient varies with temperature according to equation 3-6:

$$D = D_o \exp\left(-\frac{Q}{RT}\right) \quad (3-6)$$

Q (kJmol<sup>-1</sup>) is the activation energy for diffusion. The experiment was conducted at 15V (voltage considerably higher than the overpotential for diffusion which was around 5V for the rotations applied at ambient conditions).

However, it is not possible to conclude that the increase in current was exclusively a consequence of the increase in the diffusion coefficient due to the temperature. The electron transfer rate might have been altered and there is no guarantee that the process was under pure mass transport control for the range of temperatures of the experiment.

### 3.7. Experiments Varying Concentration of Cl<sup>-</sup> Anions

Figure 3-10 from Fushimi et al. [28] shows a Levich plot of the limiting current as a function of the square root of the rotation. In concentrated solutions ( $C_{Cl} > 0.75 \text{ mol dm}^{-3}$ ), the value of  $i_{\text{limit}}$  is proportional to  $w^{1/2}$  at small velocities, indicating that electro-dissolution of titanium is under mass transfer condition. However, a linear relation is not found at large velocities and the lines do not intersect the origin in diluted solutions ( $C_{Cl} \leq 0.75 \text{ mol dm}^{-3}$ ). This suggests that the rate-determining step of the dissolution involves some processes other than mass transfer, such as charge transfer.

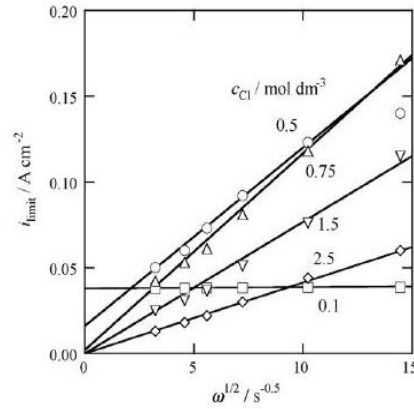


**Figure 3-10 - Potential-Independent Current  $i_{\text{limit}}$  as a Function of Square Root of Angular Velocity in LiCl Ethylene Glycol Solution [28].**

In order to distinguish the contributions of mass transport and electron transfer a Koutecky-Levich plot was obtained from the previous data.

The Koutecky-Levich equation is as follows:

$$\frac{1}{j} = \frac{1}{j_{\infty}} + \frac{1}{j_{\infty}} \times \frac{\text{Cons}}{w^{0.5}} \quad (3-7)$$

$j_{\infty}$  is defined as the current in the absence of any mass transport effects. This is an ideal situation, requiring that there were no differences between the concentrations at the bulk and electrode regardless of how fast the electron transfer is. If this value is very large, then the equation will pass through the origin. According to Figure 3-11, for concentrations below  $0.75 \text{ mol}\cdot\text{dm}^{-3}$ , the straight lines do not cross the origin, meaning that the charge transfer is not fast enough to have a pure diffusion controlled dissolution.

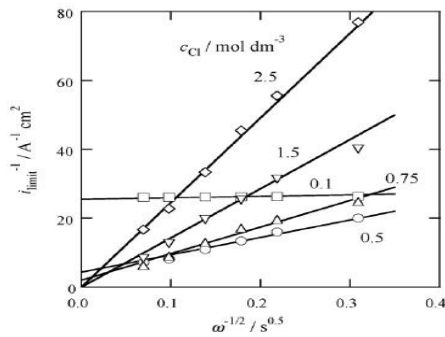


**Figure 3-11- Koutecky-Levich Plot,  $i_{\text{limit}}^{-1}$  as a Function of  $\omega^{-1/2}$ , in LiCl Ethylene Glycol Solution [28].**

Therefore, the process is not completely controlled by mass transport. The explanation given is the low electrolyte conductivity due to low concentrations of Cl.

Figure 3-12 shows the relation between  $j_{\infty}$  ( $i_k$  was used by Fushimi et al. in his paper), and the electrolyte conductivity  $\lambda$ . It is obvious that the  $i_k$  depends on solution conductivity rather than on the concentration and kind of salt. The charge transfer-controlling dissolution is mainly caused by an ohmic drop in solution, which can be overcome by an increase in the concentration of chloride salt in the solution.

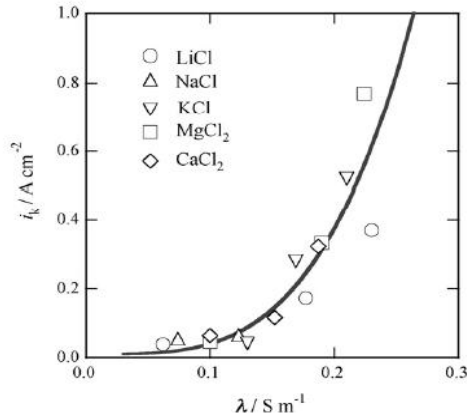


**Figure 3-12 - Relation Between Current Density in the Absence of any Mass Transfer Effect  $i_k$  and Solution Conductivity  $\lambda$  [28].**

### 3.8. Variation of the Concentration of Ti Cations in the Bulk Solution

Experiments varying the concentration of Ti cations in the solution have been made by Fushimi et al. [28]. In the case of LiCl solution containing large amounts of titanium species, the value of  $di_{\text{limit}}/dw^{1/2}$  decreases with increase in the concentration of titanium species dissolved as shown in Figure 3-13. It indicates that the titanium species dissolved at the interface also regulates its own dissolution. This is consistent with a duplex salt layer transport mechanism. The various concentrations were obtained by long polarizations of titanium in the solution.

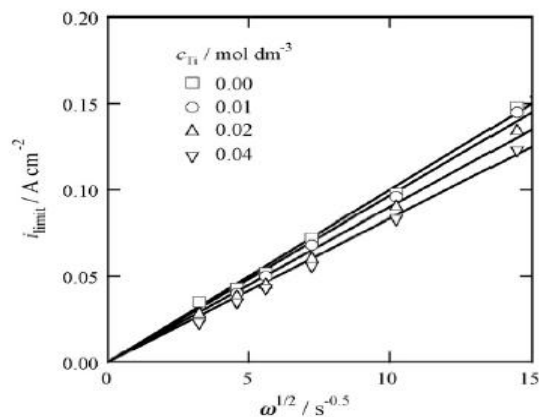


Figure 3-13 - Levich Plot in LiCl Solution Containing Different Concentrations of Ti Ions [28].

### 3.9. Roughness Analysis

Some roughness profiles have been analyzed after EP in different ways along with mechanical polishing by Fushimi et al. [17]. The results are shown in Figure 3-14 and the table below.

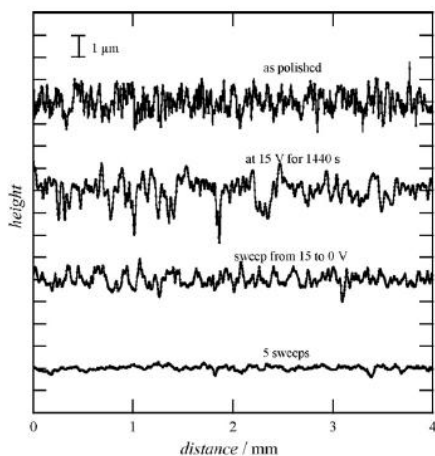


Figure 3-14 - Roughness Profiles with Different Methods [17].

Table 1  
Average roughness  $R_a$  of anodically polarized titanium electrode surfaces

Surface	$R_a$ ( $\mu\text{m}$ )
Mechanically polished	$0.364 \pm 0.003$
Anodically polished at 15 V for 30 s	$0.326 \pm 0.003$
Anodically polished at 15 V for 1440 s	$0.405 \pm 0.003$
Dynamically polarized from 15 V to 0 V	$0.228 \pm 0.003$
Five times repetition of dynamic polarization	$0.080 \pm 0.003$

These results could be reproduced in the present work (Figure 3-15). These were done with 8 sweeps going from 15V to 0V at a rate of  $10\text{mVs}^{-1}$ .

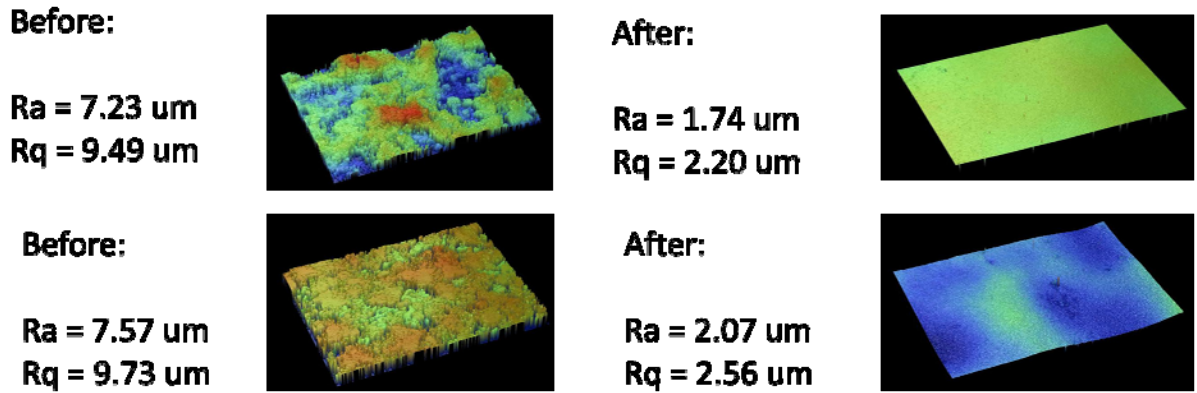


Figure 3-15 - Roughness Profiles Before and After Electropolishing.



Figure 3-16 - Titanium Piece with Tip Electropolished.

Figure 3-16 shows a picture of a titanium piece electropolished with the tip being exposed to the electrolyte while the remaining part was covered by a PTFE tape. It is possible to notice by the picture that there was material loss due to anodic dissolution along with an improvement of the surface finish.

## **4. Application of the Pulse Technology**

In this chapter, the application of electric pulses in the micro second range is investigated. The theoretical analysis done in chapter 2 suggests that the use of electrical pulses as opposed to direct current should be more effective and offer better results. The development of an apparatus to enable an inert environment to avoid oxide layer formation during the low level voltage of the pulse was necessary, and its functionality will be explained. During the course of this study, multiple experiments were made varying some of the main parameters.

#### 4.1. Formation of the Oxide Layer under Normal Conditions

The first experiments made by using the pulse technology were not successful. Instead of effective polishing, the surface of the work piece remained rough, similar to initial conditions and normally a change in color occurred. Pictures of the unsuccessful polished pieces are shown in Figure 4-1.

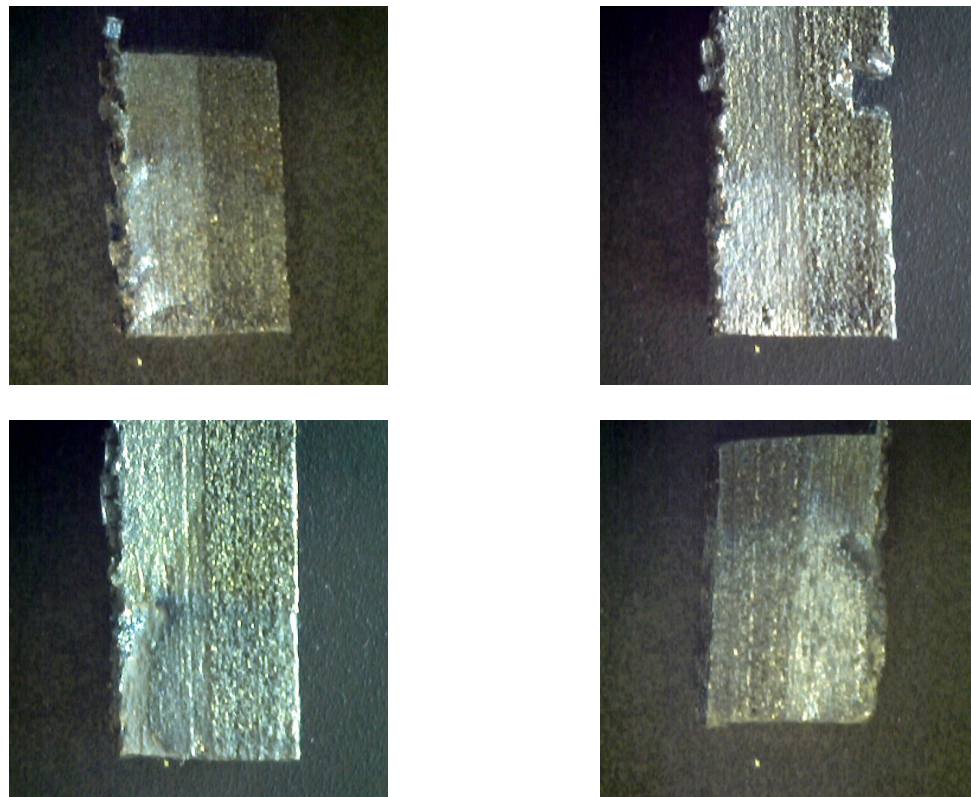


**Figure 4-1 - Ti not Successfully Electropolished with Pulse Technology due to High Oxygen Levels.**

The most probable reaction happening in this process was the increase of the oxide layer which, depending on its thickness, changes the color of the surface [33]. But this raised a question as to the source of the oxygen. Two possibilities emerged: (1) oxygen dissolved inside the ethylene glycol or (2) the oxygen came from the hydroxyl compounds.

Experiments were made injecting argon gas to mechanically expel all the dissolved oxygen in case of the first possibility. Results pointed to effective polishing which led to the development of an apparatus to control oxygen levels.

#### **4.2. High Level Temperature Issue**

It has been verified that at high electrolyte temperatures, typically values above 310K, the process fails due to undesirable reactions taking place. This has been suggested by Masatoshi Sakairi [34] while working with the same electrolyte solution but with direct current. Problems have been encountered with high temperatures since the electrolyte solution gets dark and some of the dark material gets deposited on the surface of the work piece. Figures 4-2 through 4-8 show pictures of the process with two different set-ups. The pictures on the right of each figure have a work piece with higher surface area being exposed to the electrolyte. This leads to higher currents which results in higher temperatures. Each figure compares side by side both setups at the exact time after the process started. The reactions occurring, which lead to darkening of the solution, have yet to be identified.

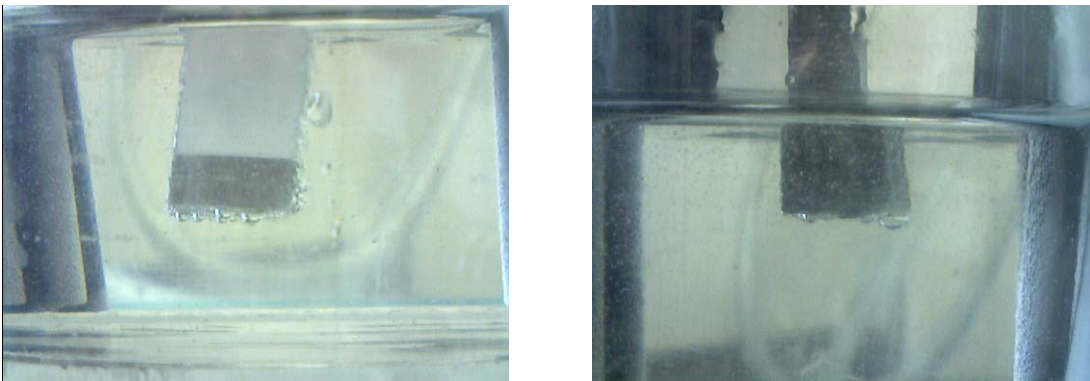


**Figure 4-2 - Side by Side Comparison of the Process with Two Different Setups. The Setup of the Right Leads to Higher Temperatures. Both Pictures were Taken at the Very Beginning of the Process.**

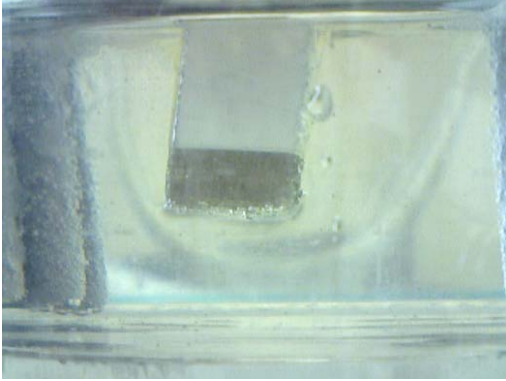


**Figure 4-3 - Identical Comparison of Figure 4-2 but 100 Seconds After.**

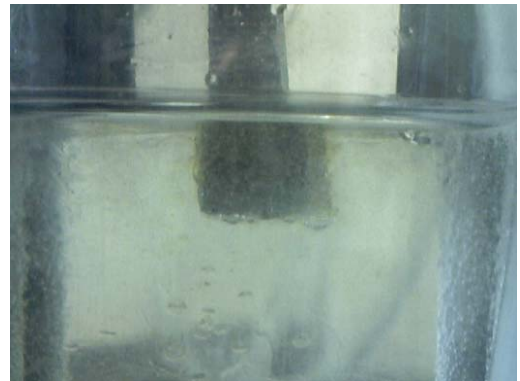
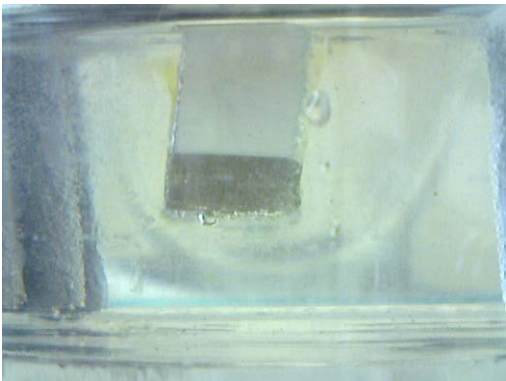


**Figure 4-4 - Identical Comparison of Figure 4-2 but 200 Seconds After.**

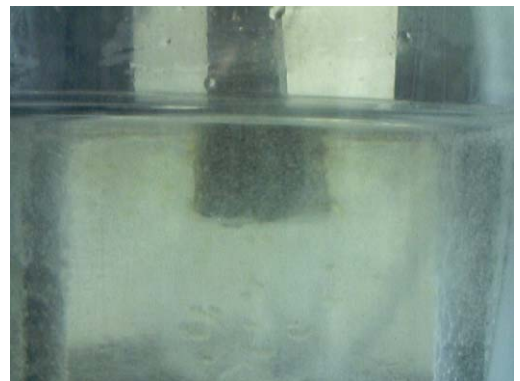
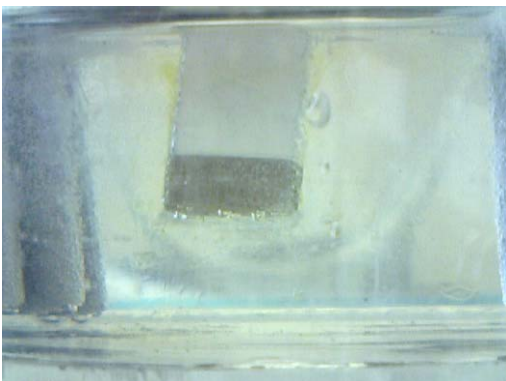


**Figure 4-5 - Identical Comparison of Figure 4-2 but 300 Seconds After.**

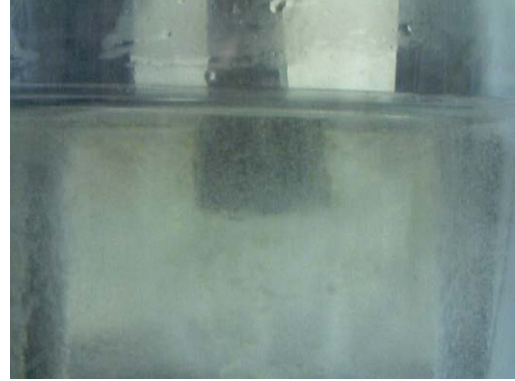
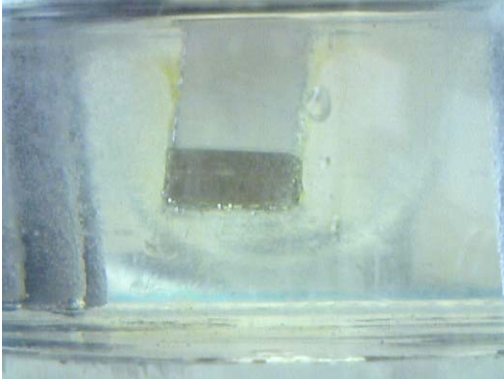


**Figure 4-6 - Identical Comparison of Figure 4-2 but 400 Seconds After.**

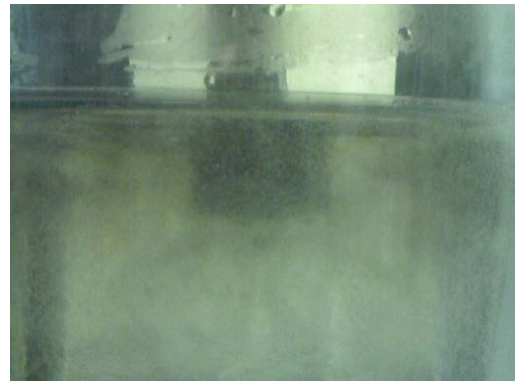
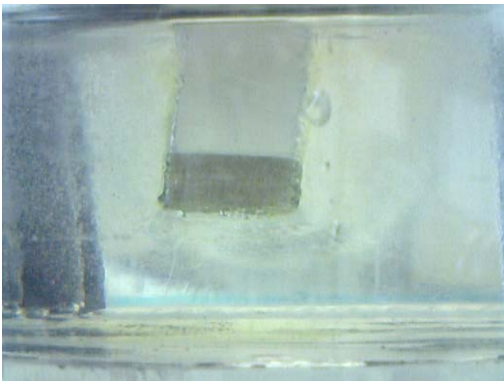


**Figure 4-7 - Identical Comparison of Figure 4-2 but 500 Seconds After.**

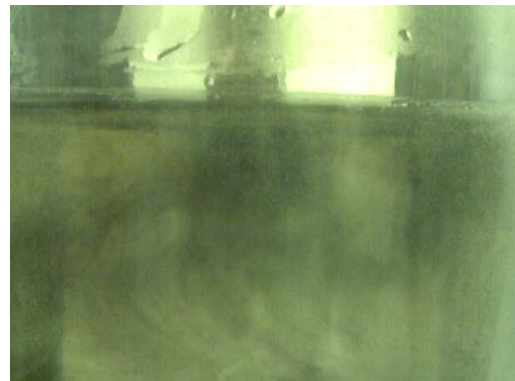
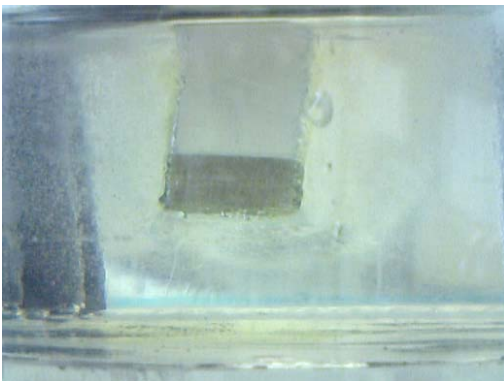


**Figure 4-8 - Identical Comparison of Figure 4-2 but 600 Seconds After.**

Figure 4-9 illustrates the net result of polishing failure due, most likely, to high temperatures.

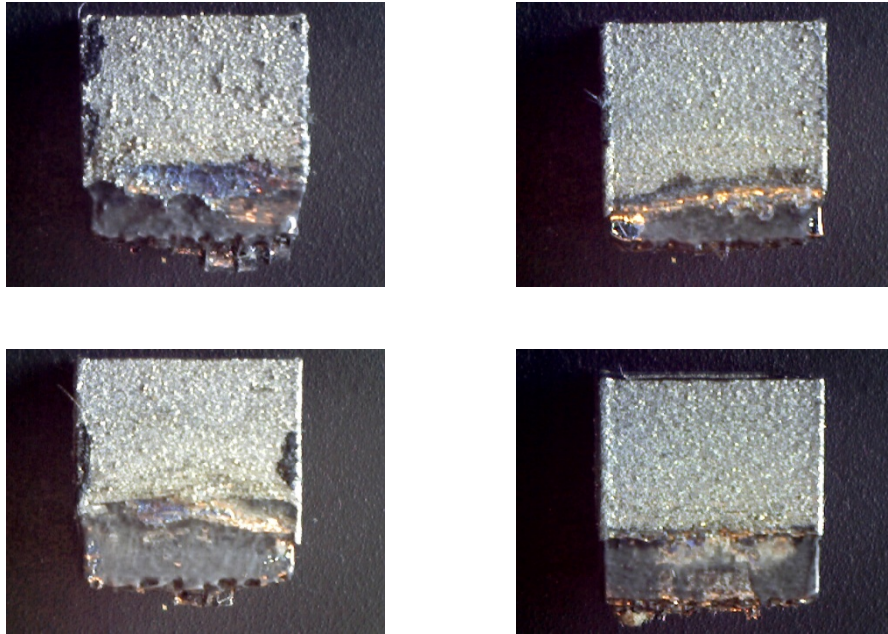


**Figure 4-9 - Ti not Successfully Electropolished with Pulse Technology due to High Temperature Levels.**

#### **4.3. Apparatus to Create an Inert Environment and Monitor Key Process Variables**

A new electrochemical cell was designed and manufactured for the purpose of optimizing the process. It enables a closed environment, permits flexibility of placing the electrodes in whatever desired position and allows for several different sizes of tanks that can be used for different sizes of work pieces (Figure 4-10). A software was developed for the cell along with an input /output interface to receive instrumentation signals (Figure 4-11). The new cell enhances the knowledge of what is happening in real time by displaying values such as temperature and oxygen levels. The sensors are described in the appendix.

Besides this, an oscilloscope is used to monitor the electric voltage of the pulses and also the current passing through the cell (Figure 4-12).



**Figure 4-10 - Electrochemical Cell Designed for Polishing Ti.**

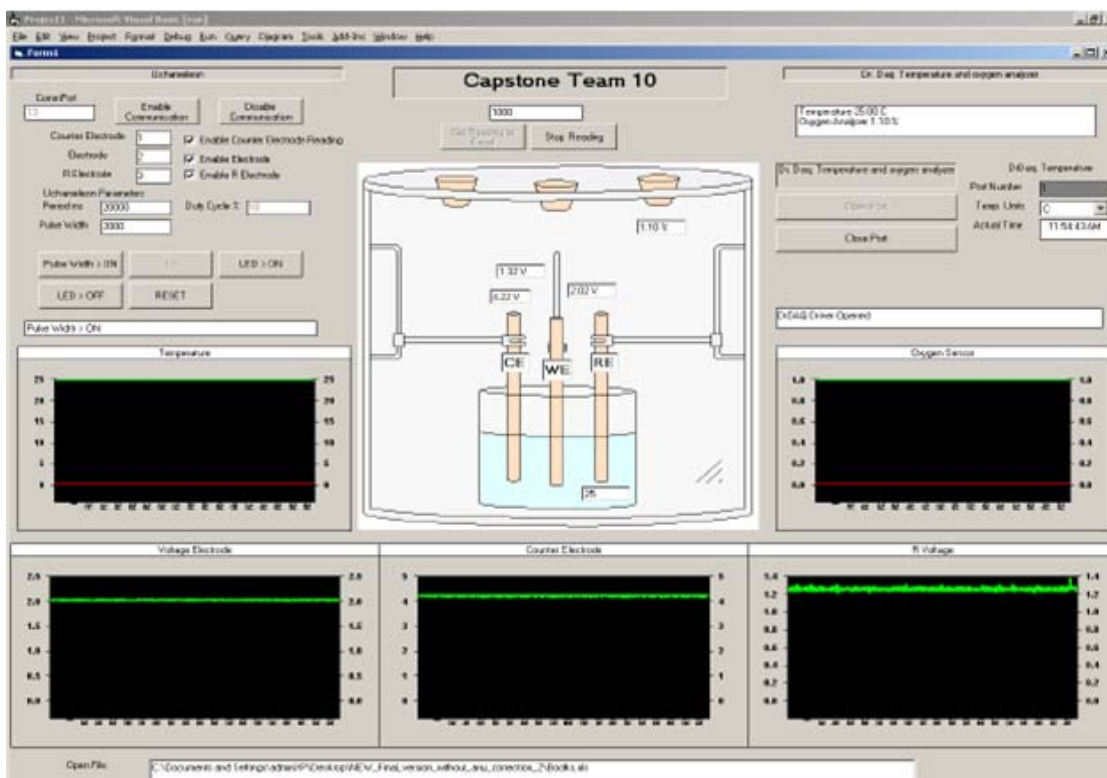
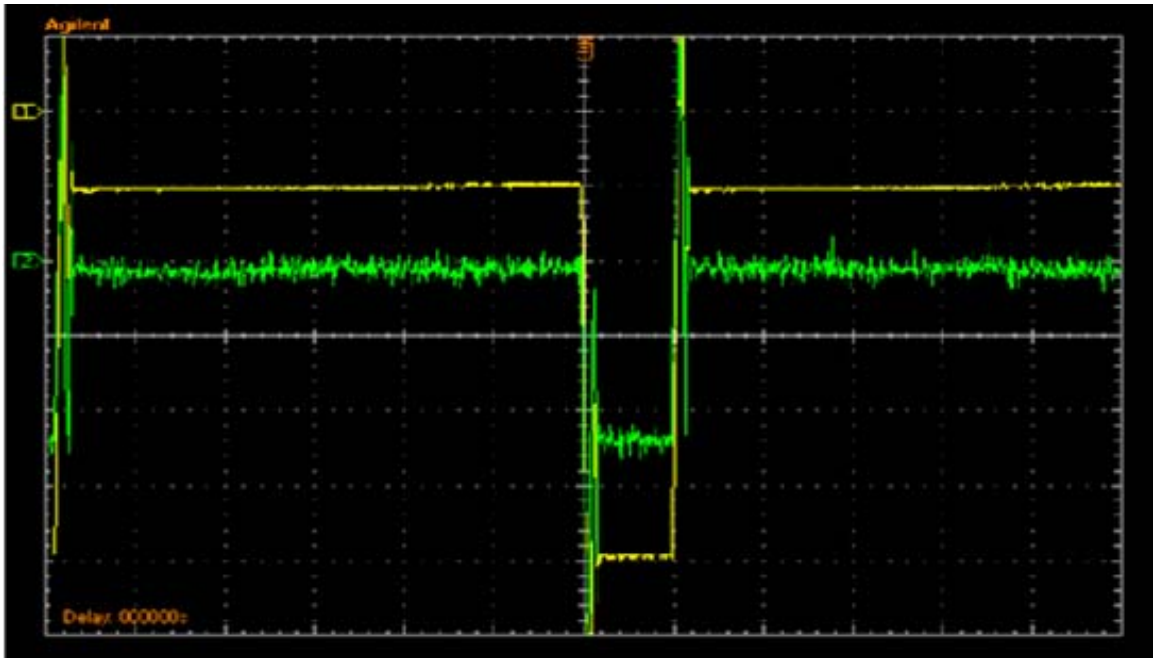


Figure 4-11 - Software Built for New Electrochemical Cell.

More details on the EP setup developed are given in the appendix.



**Figure 4-12 - Voltage and Current Values Monitored While Applying Electrical Pulses.**

#### **4.4. Results Obtained**

Good results have been obtained while applying the electric pulses with oxygen levels below 0.5% and temperatures below 310K. The electric pulses had upper voltage levels of 30V and lower voltage levels of 5V with duty cycles ranging from 15% to 50% and pulse widths from 50 $\mu$ s to 500 $\mu$ s. The electrolyte solution used was 1M NaCl-Ethylene Glycol. Graphite rods were used as counter electrodes.

Pictures of the results are shown in Figure 4-13. Only the lower section of the parts was polished while the upper sections were not exposed to the electrolyte solution.

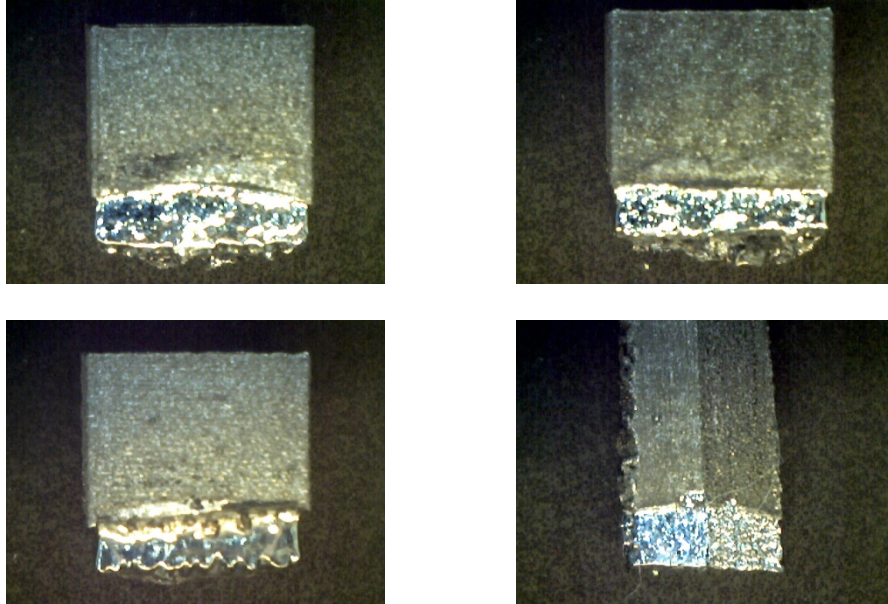


**Figure 4-13 - Titanium Pieces Successfully Electropolished with the Pulse Technology.**

A comparison between the pulse technology and direct current was made. Results measured from an optical profilometer are illustrated in Figures 4-14 and 4-15. The range of colors goes from 120 $\mu\text{m}$  to 0 $\mu\text{m}$ .

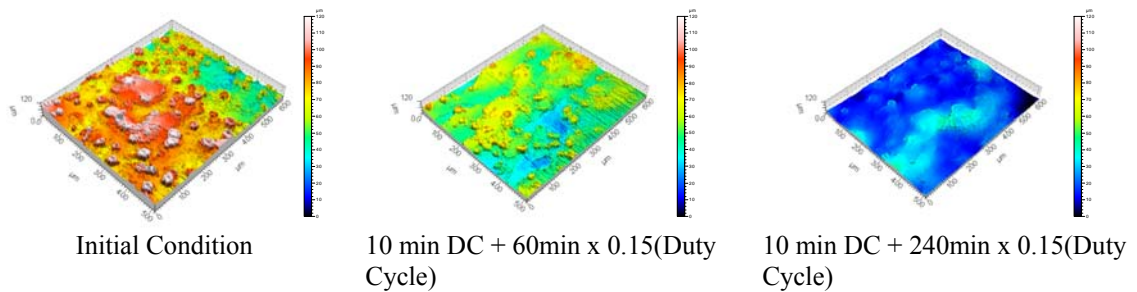


**Figure 4-14 - Roughness Profiles of Titanium Electropolished with Direct Current. The Range of Colors Varies from 120 $\mu\text{m}$  to 0 $\mu\text{m}$ .**

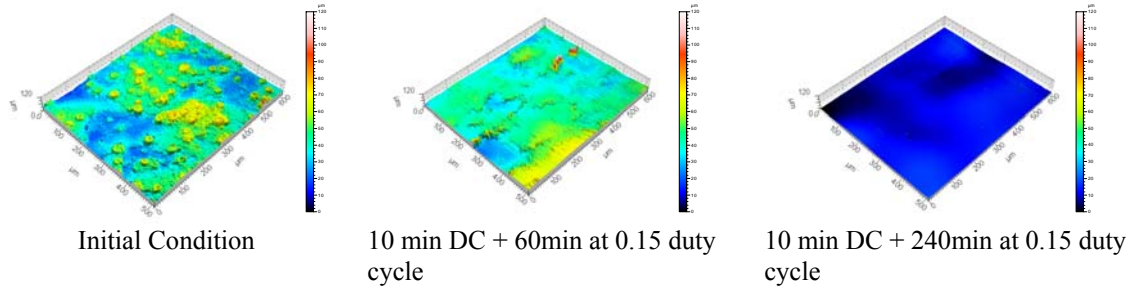


**Figure 4-15 - Roughness Profiles of Titanium Electropolished with Pulse Technology. The Range of Colors Varies from 120 $\mu$ m to 0 $\mu$ m.**

The figures above show that, as proposed by the simulation, the pulse technology is more effective to polish spherical shaped roughness in the micrometer scale.

The samples used in the experiments above are shown side by side in Figure 4-16. The stripes indicate the parts that have been polished. The amount of time increases from bottom to top and are the same for both work pieces. The left sample was polished with direct current while the right was polished with the pulse technology. The images of Figures 4-14 and 4-15 were taken from the left and right samples in Figure 4-16 respectively.

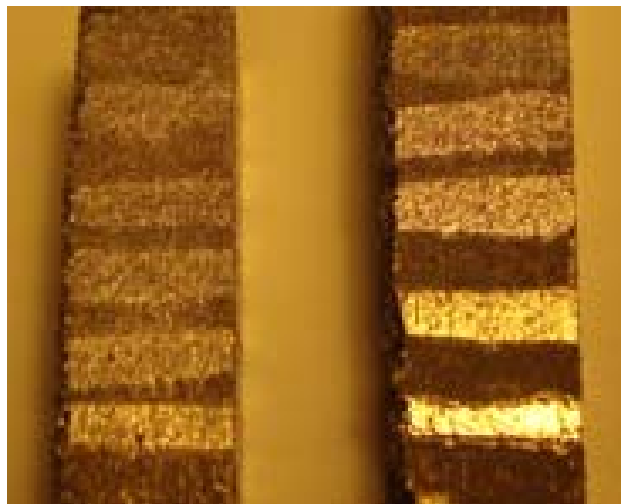


**Figure 4-16 - Samples Used for Comparison Between Direct Current and Pulse Technology.**

#### 4.5. Variation of Time

Experiments were made varying the time that the work piece was exposed to the process. Images of the results are shown in Figure 4-17. The range of colors goes from 120 $\mu\text{m}$  to 0 $\mu\text{m}$ .

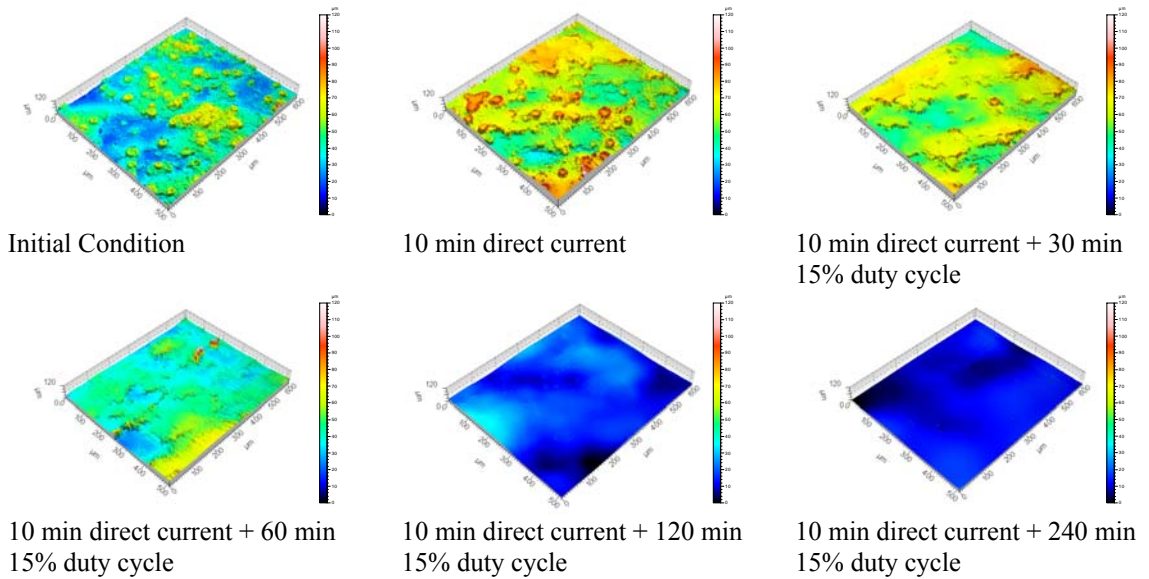


**Figure 4-17 - Roughness Profiles of Titanium Electropolished with Pulse Technology Varying Time. The Range of Colors Varies from 120 $\mu\text{m}$  to 0 $\mu\text{m}$ .**

The graph below shows the surface roughness versus the time exposed to the process. It suggests that the roughness decreases asymptotically. This makes sense since the dissolution ratio between bigger asperities and smaller asperities decreases while the surface gets smoother.

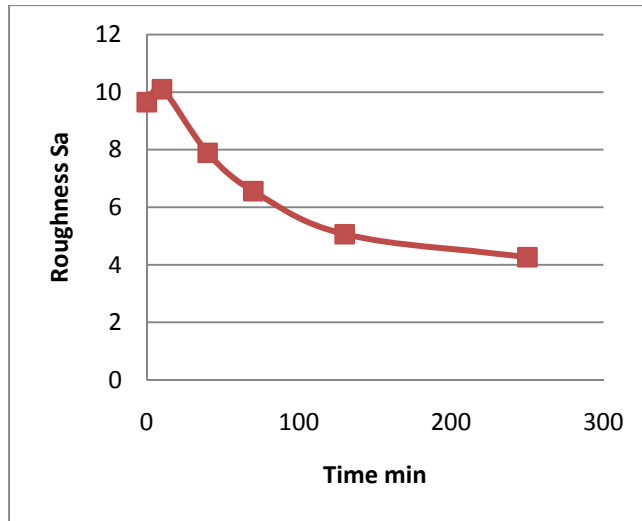
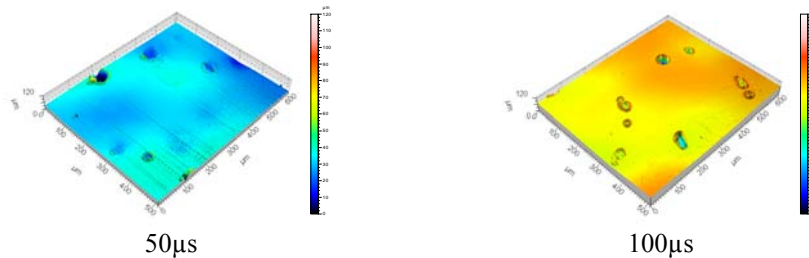


**Figure 4-18 - Variation of Surface Roughness x Time.**

The experiments suggest that 4 hours is an optimal time for the process. After this period, the amount of metal removal per surface roughness improvement would be very high.

#### **4.6. Variation of Pulse Width**

The variation of the pulse width has also been investigated. Images of the work piece being exposed to different pulse widths are shown in Figure 4-19. The range of colors goes from 120 $\mu\text{m}$  to 0 $\mu\text{m}$ .



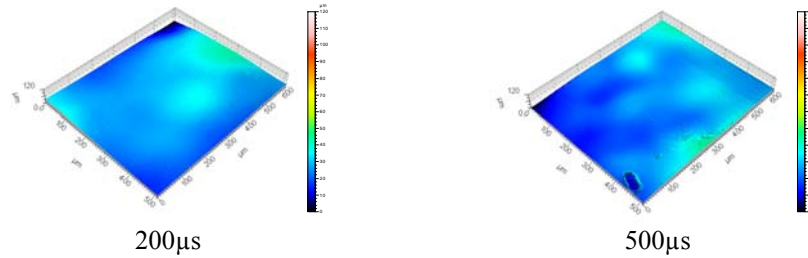


**Figure 4-19 - Roughness Profiles of Titanium Electropolished with Pulse Technology Varying Pulse Width. The Range of Colors Goes from 120µm to 0µm.**

The initial condition of the surface was also measured and is shown in Figure 4-20.

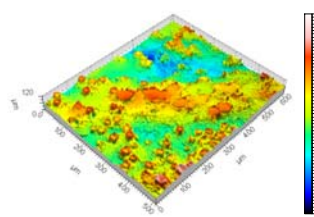


**Figure 4-20 - Initial Condition for Experiments Varying Pulse Width. The Range of Colors Goes from 120µm to 0µm.**

The sample used in the experiments above is shown in Figure 4-21. The four stripes indicate the parts that have been polished where the images were taken in Figure 4-19. The pulse width increases from top to bottom. The measured Sa of the unpolished portion of the piece was 13,3.

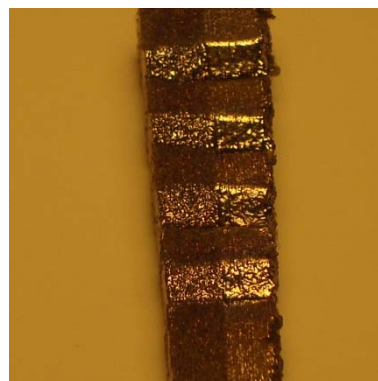


**Figure 4-21 - Sample Used for Comparison Between Pulse Widths.**

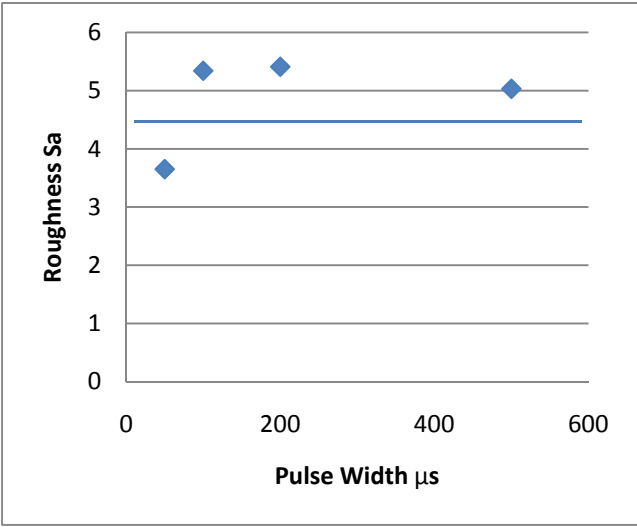


Figure 4-22 - Variation of Surface Roughness x Pulse Width.

**4.7. Variation of Duty Cycle**

The variation of the duty cycle has also been investigated. Images of the work piece being exposed to different duty cycles are shown in Figure 4-23. The range of colors goes from 210 $\mu\text{m}$  to 0 $\mu\text{m}$ .

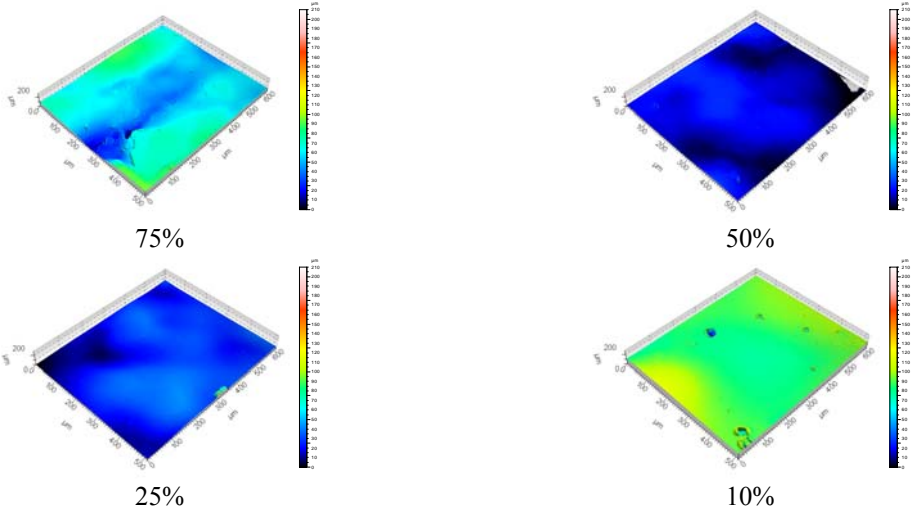
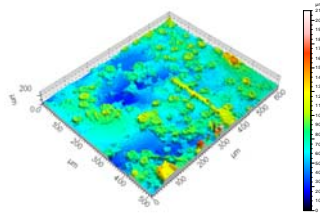


Figure 4-23 - Roughness Profiles of Titanium Electropolished with Pulse Technology Varying Duty Cycle. The Range of Colors Goes from 210 $\mu\text{m}$  to 0 $\mu\text{m}$ .

The initial condition of the surface was also measured and is shown in Figure 4-24. The measured Sa value for the initial condition was 15,3.



**Figure 4-24 - Initial Condition for Experiments Varying Duty Cycle. The Range of Colors Goes from 210 $\mu$ m to 0 $\mu$ m.**

The sample used in the experiments above is shown in Figure 4-25. The four stripes indicate the parts that have been polished where the images were taken in Figure 4-23. The duty cycle decreases from top to bottom.

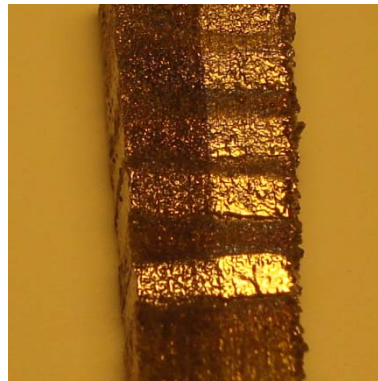


**Figure 4-25 - Sample Used for Comparison Between Duty Cycles.**

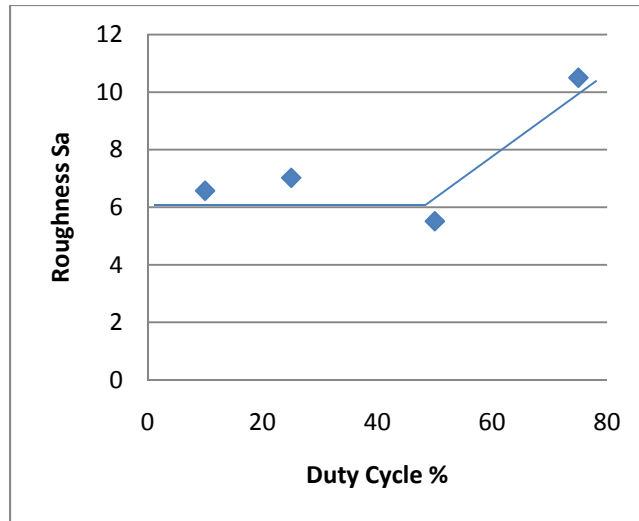


Figure 4-26 - Variation of Surface Roughness x Duty Cycle.

#### 4.8. Conclusions

The results presented in this chapter can be summarized in the following statements:

- The use of the pulse technology gives good results when electrolyte temperatures do not exceed 310K and cell oxygen levels are below 0.7%
- The results suggest that the use of the pulse technology is more effective than direct current for eliminating the asperities of the surface.
- The results suggest that the surface roughness decreases asymptotically with time exposed to the process.
- No major difference can be noticed while applying pulse widths in the range between 50 $\mu$ s and 500 $\mu$ s.
- The results suggest that lower duty cycles, 50% and below, give better results than higher ones.

## **5. Conclusions, Original Contributions to Knowledge and Future Prospects**

This chapter summarizes the investigations concerning the application of the pulse technology for the electropolishing of titanium using ethylene glycol. Ideas for future research are also presented.

### **5.1. The Pulse Technology**

The pulse technology has shown to be effective as predicted by the modeling of the Nernst diffusion layer evolution in chapter 2. Visually, the polished pieces using this technology are more shiny than the ones which were subject to the process under direct current. Analysis using an optical profilometer shows that the pulse technology is more effective in eliminating larger asperities leading to surface finish improvement.

No significant difference has been noticed while varying the pulse width between  $50\mu\text{s}$  and  $500\mu\text{s}$ . The duty cycle shows a decrease in performance while using values higher than 50%. Results varying the amount of time show that the work piece continues to improve until the highest amount of time tested which was 4 hours at a 15 duty cycle.

## **5.2. Conclusions and Original Contributions to Knowledge**

The main contributions of this thesis are categorized as follows:

- Introducing a systematic procedure for 3D polishing of titanium
- Proposing the use of the pulse technology for the process
- Describing the equations that model the Ti dissolution using the pulse technology
- Establishing an electropolishing set-up for the process
- Proposing possible chemical reactions for the process
- Identifying conditions under which the process is done successfully
- Achieving higher reductions in profilometer readings compared to results advertised by specialized companies for other materials (75% reduction as opposed to 50%) and great potential for more improvement.

### **5.3. Ideas for Future Work**

Listed below are possible subjects for students aimed at improving our comprehension of the chemistry and physics involved in the electropolishing of titanium materials using ethylene glycol as well as our comprehension of some key variables influencing yield and results of the process.

- Chemical analysis of the by-products of the process
- Use of a shaker for the work electrode during intervals of the process to avoid bubble or any other undesirable accumulation on the surface
- Investigation of the influence of current distribution
- Statistical analysis of some process parameters such as voltage, temperature, duty cycle and pulse width.

## References

- [1] F. Svahn, Å. Kassman-Rudolphi, E. Wallén, The influence of surface roughness on friction and wear of machine element coatings, *Wear* 254 (2003) 1092-1098.
- [2] E. Arslan, Y. Totik, E. Demirci, A. Alasaran, Influence of Surface Roughness on Corrosion and Tribological Behavior of CP-Ti After Thermal Oxidation Treatment, *Journal of Materials Engineering and Performance* 19 (2010) 428-433.
- [3] M. Barbour, D. O'Sullivan, H. Jenkinson, D. Jagger, The effects of polishing methods on surface morphology, roughness and bacterial colonisation of titanium abutments, *Journal of Materials Science: Materials in Medicine* 18 (2007) 1439-1447.
- [4] M. Quirynen, C.M.L. Bollen, W. Papaioannou, J.V. Eldere, D.V. Steenberghe, The Influence of Titanium Abutment Surface Roughness on Plaque Accumulation and Gingivitis: Short-Term Observations, *Int. J. Oral Maxillofac. Implants* 11 (1996) 169.
- [5] R. Osadchuk, W.P. Koster, J.F. Kahles, Recommended Techniques for Polishing Titanium for Metallographic Examination, *Met. Prog.* 64 (1953) 129.
- [6] M.J. Blackburn, J.C. Williams, The Preparation of thin foils of Titanium Alloys, *Trans. Met. Soc. AIME* 239 (1967) 287.
- [7] J.B. Mathieu, H.J. Mathieu, D. Landolt, Electropolishing of Titanium in Perchloric Acid-Acetic Acid Solution, *J. Electrochem. Soc.* 125 (1978) 1039-1043.
- [8] W.C. Coons, L.R. Iosty, Electrolytic polishing system for space age materials, *Met. Prog.* 110 (1976) 36.
- [9] J. Pelleg, Electropolishing of Ti Metallography 7 (1974) 357.
- [10] O. Piotrowski, C. Madore, D. Landolt, Electropolishing of titanium and titanium alloys in perchlorate-free electrolytes, *Plat. Surf. Finish* 85 (1998) 115.
- [11] O. Piotrowski, C. Madore, D. Landolt, The Mechanism of Electropolishing of Titanium in Methanol-Sulfuric Acid Electrolytes, *J. Electrochem. Soc.* 145 (1998) 2362.
- [12] C.R. Deckard, *Method And Apparatus For Producing Parts By Selective Sintering*, US7545142 (1991).
- [13] *SLS*, 2011 (2011).
- [14] A. Bard, *Standard Potentials in Aqueous Solutions*, M. Dekker 1985.
- [15] W. Latimer, *Oxidation Potentials*, Prentice-Hall 1952.

- [16] Y. Fovet, J. Gal, F. Toumelin-Chemla, Influence of pH and fluoride concentration on titanium passivating layer: stability of titanium dioxide, *Talanta* 53 (2001) 1053-1063.
- [17] K. Fushimi, H. Habazaki, Anodic dissolution of titanium in NaCl-containing ethylene glycol, *Electrochim. Acta* 53 (2008) 3371-3376.
- [18] J. Nguyen, G. Martin, R. Carpio, M. Grief, S. Joshi, Performance Comparisons Of Abrasive Free And Abrasive Containing Slurries For Cu/low-k Cmp, *Materials Research Society* 732E (2002) I1.4.1.
- [19] *Fladder Deburring System*, 2011 (2011).
- [20] Y. Uno, A. Okada, K. Uemura, P. Raharjo, S. Sano, Z. Yu, et al., A new polishing method of metal mold with large-area electron beam irradiation, *J. Mater. Process. Technol.* 187-188 (2007) 77-80.
- [21] V. Palmieri, Fundamentals of Electrochemistry - The Electrolytic Polishing of Metals: Application to Copper and Niobium, *Proceedings of the 11th Workshop on RF Superconductivity* (2003) 579.
- [22] R.L. Davi, An electropolishing primer, *Products Finishing* (1995) 68-71.
- [23] D. Landolt, Fundamental aspects of electropolishing, *Electrochim. Acta* 32 (1987) 1-11.
- [24] W.J. McTegart, *The Electrolytic and Chemical Polishing of Metals*, 1956.
- [25] M. Matlosz, Modeling of impedance mechanisms in electropolishing, *Electrochim. Acta* 40 (1995) 393-401.
- [26] M. Abramowitz, I.A. Stegun, *Handbook of Mathematical Functions With Formulas, Graphs, and Mathematical Tables*, NBS Applied Mathematics Series 55 ed., National Bureau of Standards 1964.
- [27] T. Deguchi, K. Chikamori, Development of Electropolishing Method of Titanium Materials, *Proceedings of the 2003 Annual Meeting of the Japan Society for Precision Engineering* (2003) 338.
- [28] K. Fushimi, H. Kondo, H. Konno, Anodic dissolution of titanium in chloride-containing ethylene glycol solution, *Electrochim. Acta* 55 (2009) 258-264.
- [29] F. Bonet, C. Guéry, D. Guyomard, R. Herrera Urbina, K. Tekaia-Elhsissen, J.-. Tarascon, Electrochemical reduction of noble metal species in ethylene glycol at platinum and glassy carbon rotating disk electrodes, *Solid State Ionics* 126 (1999) 337-348.
- [30] D.R. Lide, *Handbook of chemistry and physics CRC*, 87th ed. 2007.

[31] M. Li, Y. Chen, An investigation of response time of TiO<sub>2</sub> thin-film oxygen sensors, *Sensors Actuators B: Chem.* 32 (1996) 83-85.

[32] S. Veltman, T. Schoenberg, M.S. Switzenbaum, Alcohol and acid formation during the anaerobic decomposition of propylene glycol under methanogenic conditions, *Biodegradation* 9 (1998) 113.

[33] G. Jerkiewicz, B. Zhao, S. Hrapovic, B.L. Luan, Discovery of Reversible Switching of Coloration of Passive Layers on Titanium, *Chemistry of Materials* 20 (2008) 1877-1880.

[34] M. Sakairi, M. Kinjyo, T. Kikuchi, Optimization of Environment-friendly Electrochemical Polishing Process for Titanium Plate Electrode,.

## **Appendix**

### **1. CONTROL SYSTEM AND ELECTRONIC COMPONENTS**

#### **1.1 Selection of Controllers**

The setup uses several electronic components to monitor and/or control current, temperature and oxygen levels. These components include sensors, controllers and a computer for sending commands to the controllers and displaying experimental results. Two separate controllers were chosen. The first one is the  $\mu$ Chameleon I/O interface board (shown in Figure 1). It is a highly flexible board that is capable of outputting both direct and pulsed currents of 5V at a maximum frequency of 5 MHz through several of its pins. Other pins can also be programmed to read voltage inputs of 0 to 5V coming from external circuits. The device has the added benefit of being able to be powered and controlled entirely by a computer's USB port. Table 1 shows the function of each pin on the device.

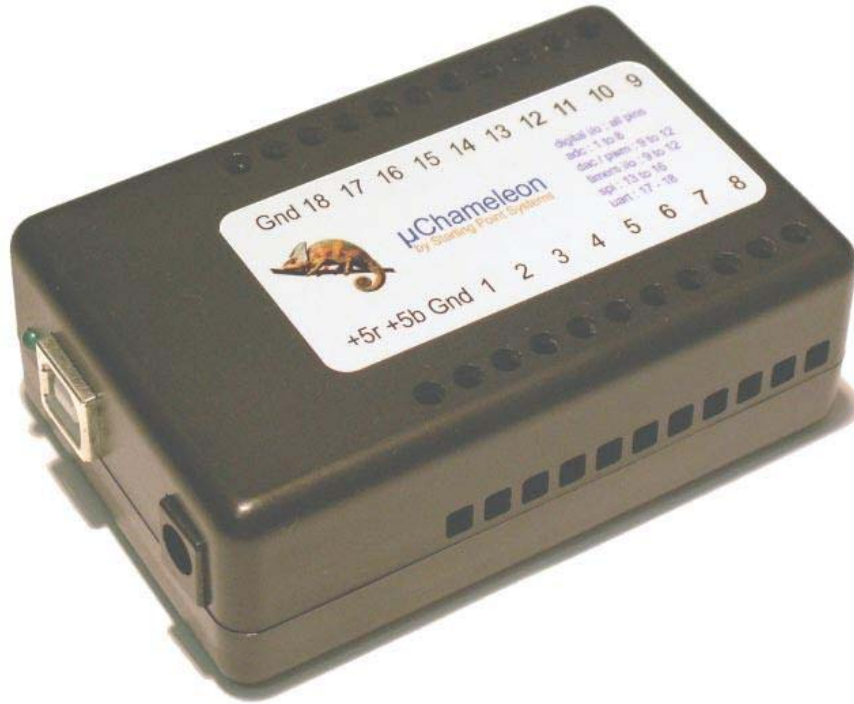


**Figure 1 - µChameleon I/O Interface Board [W2]**

<b>Special function</b>	<b>Applicable pin numbers</b>
digital i/o all pins	all pins
analog inputs	1 to 8
analog outputs	9 to 12
timers	9-12

**Table 1 - µChameleon Pin Functions**

The other controller used in the setup is the DrDAQ data acquisition board (shown in Figure 2). It is capable of reading inputs from a multitude of external sensors including

temperature probes and oxygen analysers. It is powered and controlled from the computer's parallel port.



**Figure 2 - DrDAQ Data Acquisition Board [W3]**

The selection of these two devices was based on the number and types of inputs/outputs they have, their availability in the lab, and the programming languages they support. They are both fully compatible with the Visual Basic 6.0 (VB6) programming environment and can thus receive commands from Microsoft Windows-based machines. VB6 was chosen for its ease of use.

## **1.2 Sensors**

The two sensors used for the apparatus are a temperature probe and an oxygen sensor. The temperature sensor is a Resistance Temperature Detector (shown in Figure 3) and has a range of -10 to 105 °C with a resolution of 0.1 °C. The oxygen sensor (shown in

Figure 4) is of the galvanic cell type and has a range of 0-100% oxygen with an accuracy of 1 %. Both of these are connected to the external sensor ports of the DrDAQ device.



**Figure 3 - Temperature Sensor [W4]**



**Figure 4 - Oxygen Sensor [W5]**

### **1.3 Current Control and Monitoring System**

The most important process variable for the setup is the current that passes through the workpiece. The generation of a periodic current is achieved through the  $\mu$ Chameleon's timer pin 9, which has been programmed to output a Pulse Width Modulated (PWM)

voltage (shown in Figure 5). The width and period of this voltage can be directly selected by the experimenter up to a maximum frequency of 5 MHz. The  $\mu$ Chameleon can only output 5 V through the PWM output, so the voltage is first passed through an analogue attenuator (shown in Figure 6) that can lower it to a desired value. Then, the voltage is fed to a potentiostat already present in the lab and amplified with a gain of 10 (shown in Figure 6), after which it is finally applied to the workpiece and electrode. This design allows for a PWM voltage of 0-50 V and fully meets the electrical current requirements of the setup.

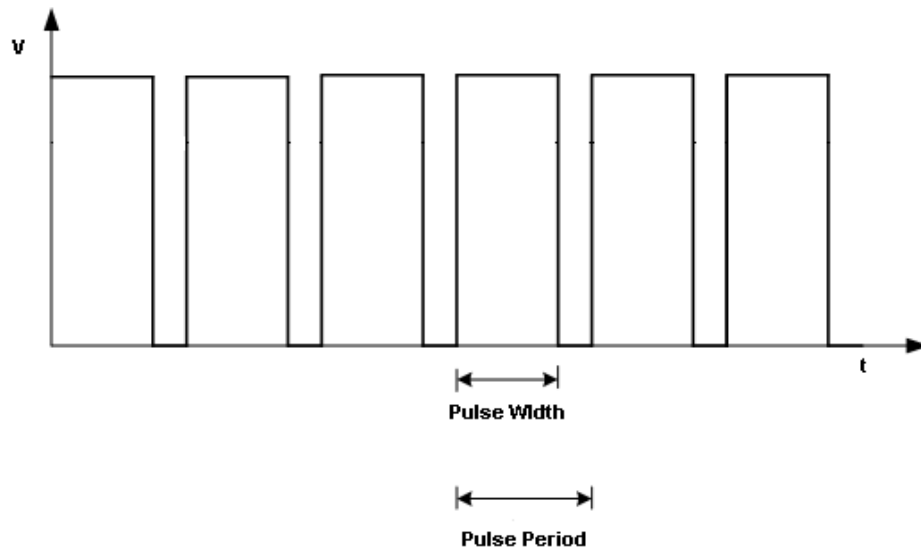


**Figure 5 - Generic PWM Pulse**



**Figure 6 - Voltage Attenuator (left) and Potentiostat (right)**

The applied voltage creates a current whose strength is proportional to the resistance of the workpiece. For the setup, the maximum current allowed by the potentiostat is 5 A. The current is continuously monitored by placing a resistor in series with the wire connecting the potentiostat to the workpiece, by measuring the voltage drop across it using an oscilloscope and then by converting this voltage to a current value. The resistor that is used has a very low resistance value (0.1 ohms) so that the voltage drop across it remains small enough to be read by the oscilloscope.

The actual current flowing through the resistor (and hence the workpiece) is finally found from the following relationship:

$$I = \frac{V}{R}$$

The electronic components of the apparatus have been placed in a plastic open-top box for simplicity and organization, as shown in Figure 7.

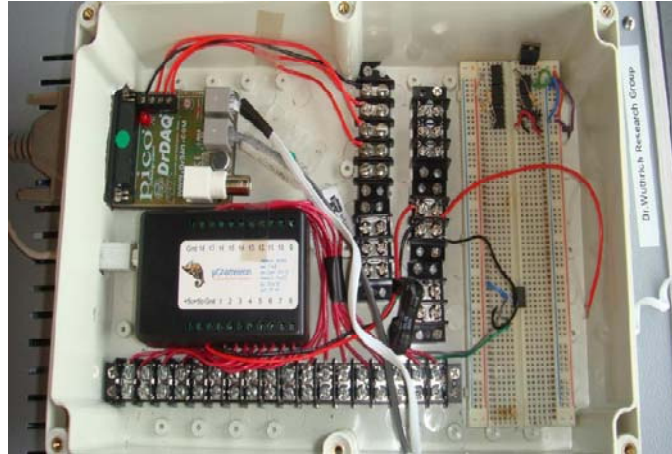


**Figure 7 - Electronic Assembly**

## **2. PROGRAMMING AND GRAPHICAL USER INTERFACE**

Programming is a very important aspect of the apparatus. It allows for the user to control and monitor several of the process parameters. For this purpose, a graphical user interface (GUI) has been coded.

### **2.1 Graphical User Interface**

The GUI used for the setup, as shown in Figure 8, has several components to its functioning. Its main feature is that it allows the user to precisely control the PWM voltage by specifying its period and width. It can also display not only the RMS voltage coming from the potentiostat, but also the voltage at up to two electrodes, should they be connected to the input pins 2 and 3 of the uChameleon board. There is a button included

to reset the uChameleon in case it malfunctions and another button to end the voltage output. Two other buttons turn the LED indicator on the device on and off, and they can be used by the user to determine if it is responding to commands. Then, oxygen levels in the tank are displayed as well the electrolyte temperature for which the user can select between units of degrees Celsius, Fahrenheit or Kelvin. All of the measured variables (voltage, temperature and oxygen levels) are plotted in real-time within the GUI. Finally, the software logs all of these variables to an excel file at time intervals specified by the user.

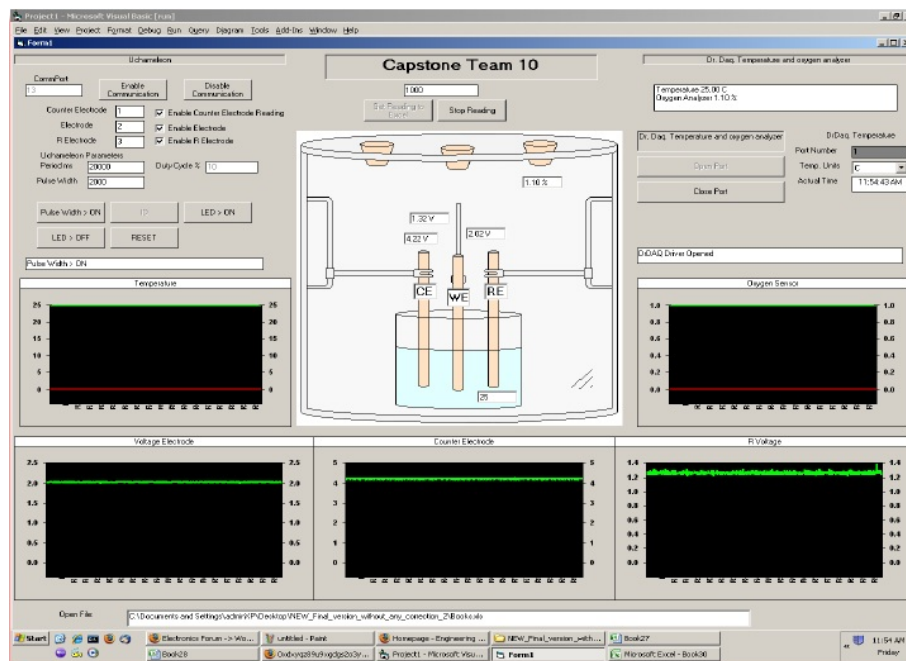


**Figure 8 - Software GUI**

The strength of the GUI resides in its ease of use and its integrated design. All of the process variables are controlled and monitored from a single interface. The logging of

experimental data also gives freedom to the experimenter to not be present during the entire experimental run, which can last up to several hours.

## **2.2 Programming Code**

The program was developed using Visual Basic 6.0. The software that has been developed communicates with the uChameleon and the DrDAQ boards through the computer's USB and parallel ports simultaneously. It has been programmed to detect the devices regardless of which port number they are connected to. The computer software and all other aspects of the design have added several benefits for the process.

## **References**

- [W1] CAMRY Instruments, "The EuroCell™ CorrosionCell", <http://www.gamry.com/Products/EuroCell.htm>, (current March 23, 2010).
- [W2] UChameleon, <http://www.starting-point-systems.com/pict0317.html>, (current March 23, 2010).
- [W3] Dr.DAQ, <http://www.drdaq.com/graphics/drdaq2.jpg>, (current March 23, 2010).
- [W4] Temperature probe, [http://www.drdaq.com/graphics/temp\\_sensor.jpg](http://www.drdaq.com/graphics/temp_sensor.jpg), (current March 23, 2010).
- [W5] Dr.DAQ, "Oxygensensor", [http://www.drdaq.com/graphics/oxygen\\_sensor.jpg](http://www.drdaq.com/graphics/oxygen_sensor.jpg), (current March 23, 2010)